Statistical Evaluation of Time Multiplexing to Mitigate Differential Reflectivity Bias Due to Cross-Polar Coupling

IGOR R. IVIĆ

Cooperative Institute for Mesoscale Meteorological Studies, University of Oklahoma, and NOAA/OAR/National Severe Storms Laboratory, Norman, Oklahoma

(Manuscript received 24 November 2014, in final form 23 June 2015)

ABSTRACT

One of the main challenges to the use of phased array radar for weather observations is the implementation of dual polarization with acceptable levels of cross-polar fields induced by the antenna. For example, to achieve acceptable differential reflectivity (Z_{DR}) bias (e.g., less than 0.1 dB) using simultaneous transmission and reception of H and V polarized waves, the isolation between coaxial cross-polar and copolar beams needs to be in excess of 50 dB. Because such isolation cannot be achieved at an affordable price by antenna hardware, additional methods are required to attain supplementary isolation of orthogonal channels. One such option is time multiplexing. Herein, this approach is evaluated from the statistical aspect, whereby the depolarization caused by the radar hardware is accounted for in this study. An evaluation is conducted using theoretical analysis as well as simulated and time series data from a weather radar. The main criteria for evaluation are the bias and standard deviation of differential reflectivity estimates. The results indicate that the implementation of the time-multiplexing method has the capability to significantly improve upon the radar intrinsic cross-polar isolation. However, it is demonstrated herein that the reflectivity gradients in range adversely affect the efficacy of the method and that the standard deviation of estimates can significantly increase as a result of the time-multiplexing application.

1. Introduction

The Weather Surveillance Radar-1988 Doppler (WSR-88D), operated by the National Weather Service, is one of the key providers of weather information for the entire United States. As such, the WSR-88D network is constantly evolving, with the most recent and significant addition to the network being dual-polarization capability. Dual polarization provides new information that improves the abilities of forecasters and algorithms to distinguish between different types of precipitation (e.g., rain, hail) and nonweather scatterers (e.g., insects, ground clutter) as well as more accurate qualitative precipitation estimation (QPE).

In recent years, phased array radar (PAR) technology has been proposed as a foundation for development of the next-generation weather surveillance systems. This technology supports more flexible scanning strategies than radars using mechanically steered antennas and has the potential to provide reduced data update times. The advantages of using PAR technology for weather observations have been discussed by Zrnić et al. (2007), and experiments demonstrating these using a single-polarized PAR are conducted at the National Severe Storms Laboratory (e.g., Heinselman and Torres 2011). The PAR technology has been principally developed to advance point target detection and tracking, but dual-polarization PAR has hardly any precedent. Notable exceptions are recently built X-band agile-beam polarimetric weather radars (Salazar et al. 2010; Knapp et al. 2011; McCarroll and McLaughlin 2012). It is certain that if PAR is to become the next-generation weather radar, it will have to include dual-polarization technology [polarimetric phased array radar (PPAR)] that meets or exceeds the current surveillance capabilities of existing weather radars (e.g., WSR-88D).

Generally, implementation of dual-polarization for weather applications imposes strict requirements on antenna design and fabrication. This is due to the nature of dual-polarization measurements, which require considerable isolation between the horizontal and vertical channels and ideally no transmission of cross-polar

Corresponding author address: Igor Ivić, National Weather Center, 120 David L. Boren Blvd., Norman, OK 73072.
E-mail: igor.ivic@noaa.gov

DOI: 10.1175/JTECH-D-14-00224.1

fields. Even perfectly fabricated reflector antennas [i.e., with no cross coupling between horizontal (H) and vertical (V) channels leading to the antenna; Jones 1954; Chandrasekar and Keeler 1993; Zrnić et al. 2010] produce cross-polar fields; that is, a portion of the energy inserted into the H antenna port is also transmitted as the cross-polar V field and vice versa. The result is that the measured echo voltages in the V channel are contaminated by the echoes caused by the H cross-polar field if the H port is solely excited and vice versa. Boresight cross-polar fields introduce the most bias in the estimates of polarimetric variables. This is because the most power of cross-polar signals originates from these fields. Also, they are collocated with the main beam so their returns are coherent with those from copolar fields. For well-designed phased array elements, cross-polar fields are minimal (ideally zero) in the principal planes of the radiation/reception patterns but are significant elsewhere (Lei et al. 2015).

The result is that the measured voltages in the V channel are contaminated by the returns caused by the cross-polar field transmitted by the H channel and vice versa. For phased array antennas, this effect is minimal if beams are directed along the principal planes but increases otherwise. In addition, the close proximity of hardware leading to the array elements can cause a portion of the energy present in the H channel to leak into the V channel, and vice versa (herein referred to as channel-to-channel cross coupling). This effect is present on both transmission and reception, resulting in the contamination of voltages measured in the H channel by the returns from vertically polarized field and vice versa. Because of high component integration, coupling through PPAR hardware (e.g., the circuits behind the antenna backplane) is even more prominent compared to radars using reflector antennas.

All polarimetric measurements are influenced by these effects. Those that are of most concern are the differential reflectivity (Z_{DR}), the copolar correlation coefficient magnitude $|\rho_{hv}(0)|$ (herein referred to as correlation coefficient), and the differential phase ϕ_{DP} (Doviak and Zrnić 1993, section 8.5.2.3). In case of Z_{DR}, it is certain that the cross-coupling effects will be compounded with other bias-inducing effects already present in radars using parabolic antennas (Hubbert et al. 2003; Zrnić et al. 2006; Ice et al. 2014). Additionally, in most planar PPAR architectures, the nonorthogonal orientation of intended H and V fields occurs when the beam is pointed away from the principal planes (Zhang et al. 2009; Zrnić et al. 2011; Lei et al. 2015). The net effect is that the amount of energy transmitted in the cross-polar H and V fields increases and the difference between the H and V copolar field powers is different for each beam position as the beam is steered away from broadside. The differences in the H and V copolar beam powers can be accounted for using calibration, whereas the effects of cross-polar fields cannot because they are dependent on the intrinsic signal parameters such as Z_{DR}, $|\rho_{hv}(0)|$, and ϕ_{DP} (Zrnić et al. 2010). Consequently, the issue of cross-polar fields must be dealt with using means other than calibration. Thus, to keep the overall bias within the desired limits, it is likely that the Z_{DR} calibration in PPAR will be an order of magnitude more difficult than in radars with parabolic antennas.

To circumvent the nonorthogonal orientation of intended H and V fields, Zhang et al. (2011) proposed a cylindrical design [cylindrical polarimetric phased array radar (CPPAR)], whereby the beam is steered in azimuth by commuting illumination of the array elements so beams are always in the vertical principal plane. Another alternative is a system where beams are electronically scanned only in one of the orthogonal principal planes and mechanically scanned in the other (Knapp et al. 2011). Finally, the use of electric and magnetic dipoles aligned in the vertical to create orthogonally polarized electric fields in all directions was proposed by Crain and Staiman (2007). With such an ideal arrangement, only copolar H or V fields are transmitted in all directions if the H or V port is excited. Nonetheless, given practical implementations, cross-polar coupling through the radar antenna and the surrounding microwave circuitry remains and must be dealt with. Because of these issues, the Multifunction Phased Array Radar Symposium II (http://www.ofcm.noaa.gov/mpar-symposium, 17–19 November 2009) identified the polarimetric capability to be the most challenging technical issue for future multimission phased array radar (MPAR).

The two typical modes of polarization implementation are the alternate (AHV) and simultaneous (SHV). In the AHV mode, the H and V ports of the antenna are alternately excited, whereas in the SHV mode ports are excited simultaneously. The polarimetric measurements in the two modes are differently affected by the cross-polar fields generated by the antenna and channel-to-channel cross coupling. For the same cross-polar isolation, the AHV is advantageous in that the Z_{DR} bias is much smaller than in the SHV mode (Sachidananda and Zrnić 1985; Wang and Chandrasekar 2006). Unfortunately, the AHV mode of operation presents numerous other challenges. The most important is that it is not compatible with the SHV mode in which the dual-polarized WSR-88D currently operates; hence, switching to the AHV mode would require significant changes in the existing algorithms. More generally, there are significant challenges with AHV mode transmission when obtaining

the dual-polarization variables with the required quality while maintaining an unambiguous range of ~300 km (Zrnić et al. 2012).

If SHV is used for the PPAR, then the current algorithms can be seamlessly transferred to the new hardware. Further, advantages of the SHV mode are 1) estimates with significantly lower errors for the same scan rates, 2) the differential phase is measured within a 360° interval, 3) the correlation coefficient can be measured directly (i.e., no need to assume a correlation model), and 4) there are no compromises in the performance of the ground clutter filter (Zrnić et al. 2012). This compels us to search for ways other than better antenna design to improve cross-polar isolation that would suit the PPAR design and enable the use of SHV mode with satisfactory Z_{DR} bias.

Orthogonal coding in the SHV mode to enable cross-polar measurements (i.e., all four elements of a target scattering matrix), without taking into account the effects of cross-polar signals, was proposed by Giuli et al. (1993) and later by Stagliano et al. (2006). In the case of Stagliano et al. (2006), the code details were not specified (see also Stagliano et al. 2009). A conceptual approach therein is to make the returns, from the transmitted fields in H and V, orthogonal by changing the phase of the transmitted waves multiple times within the pulse. This provides for separation of the copolar and cross-polar components of the backscattered signals in the H and V channels. The additional effect of doing so is that the impact of signals caused by cross-polar coupling in the SHV mode on the differential reflectivity is also diminished. Unfortunately, because the zero-lag copolar correlation coefficient $\rho_{hv}(0)$ is estimated by calculating the correlation between H and V backscattered signals, this type of orthogonal coding precludes estimation of $\rho_{hv}(0)$ from second-order estimates at zero lag as has been shown in Ivić (2013).

Chandrasekar and Bharadwaj (2009) proposed cross-polar measurements in the SHV mode by implementing phase changes on transmission from pulse to pulse using Walsh–Hadamard codes. The scheme operates by shifting the spectrum of one of the signals (H or V) by half the Nyquist interval so that after it couples with the other signal it can be removed by filtering. Consequently, such a scheme may also be used to suppress the effects of cross-polar coupling but poses the requirement that the number of samples used in estimation is a power of 2. A similar, but much simpler, scheme is proposed by Zrnić et al. (2014), whereby modulations similar to Sachidananda and Zrnić (1986) are used to achieve the same goal. To obtain the full benefit, this scheme requires the number of samples, used in estimation, to be even.

Clearly, if filtering of cross-polar signals in the spectral domain is employed, both schemes require that the Nyquist interval be large enough so that the spectra of two signals do not overlap (for the most part) so that filtering can succeed in removing unwanted cross-polar signals. However, in the current implementation on the WSR-88D, the polarimetric variables at the lowest two (sometimes three) elevation angles are obtained in the SHV mode using long pulse repetition time (over 3 ms) so that range ambiguities do not occur. Such long pulse repetition times (T_s) result in small unambiguous velocities (~9 m s^{-1}). This reduces the number of cases where the spectra of copolar and cross-polar signals are sufficiently separated to enable successful removal of cross-polar signals via spectral filtering. Nonetheless, both schemes diminish the bias in H and V power estimates even without the use of filtering. This is because they induce a pulse-to-pulse alternating positive/negative sign in the products of copolar and cross-polar signals so the estimates of these cancel each other in the mean using simple time averages of the received powers in the H and V channels.

A technique that reduces the effects of antenna cross coupling using cross-polar correlation measurements has been proposed by Galletti et al. (2014). Such measurements are readily available in the AHV mode but not in the SHV mode. These may be extracted in the SHV mode using the orthogonal codes [as described by Giuli et al. (1993) and Stagliano et al. (2009)]. However, straight application of such codes prevents estimation of $\rho_{hv}(0)$ at zero lag as noted earlier in the text. Alternatively, switching between the two orthogonal waveforms in the H and V channels [simultaneous transmission and simultaneous receive (STSR) orthogonal four-polarization pulsing scheme in Galletti et al. (2014)] allows the $\rho_{hv}(0)$ measurement from second-order estimates at one and two lag. Such an approach, however, is likely to produce lower-quality $\rho_{hv}(0)$ estimates from scans with long pulse repetition times (PRT) as a result of the insufficient correlation in sample time (e.g., surveillance scans in WSR-88D) (Ivić 2013).

Another approach proposed by Zrnić et al. (2014), to suppress cross-polar signals, is time multiplexing, in which the V transmitter port is energized immediately after the H port or vice versa. In the regular SHV mode, the estimated powers in H and V are the sums of copolar and cross-polar signal powers as well as the product of these two signals (herein referred to as the co/X-pol product). Because the copolar and cross-polar signals from weather are highly correlated, their product is the main cross-polar coupling bias contributor. Ideally, in a time-multiplexed arrangement, the copolar and cross-polar signals in H and V belong to different resolution

volumes (V_6) and are rendered uncorrelated so their product becomes zero in the mean. Thus, the estimated powers in H and V are the sums of copolar and cross-polar signal powers only. However, because copolar and cross-polar signals belong to different resolution volumes, the cross-polar power can induce a larger bias in the case of strong reflectivity gradients. If pulses in the horizontal and vertical channels are transmitted within an adequate time interval, it can be assumed that the scatterers are frozen during the period needed to acquire data from the same resolution volume in the horizontal and vertical channels. Therefore, this mode of polarimetric data acquisition is compatible with the SHV mode and can be regarded as the quasi-simultaneous HV (QSHV) mode. Consequently, time series collected using the QSHV mode can be seamlessly passed to the signal processing algorithms developed for the SHV mode. Herein, a statistical evaluation of the QSHV mode to suppress cross coupling is conducted. Throughout the paper the bias and standard deviation are the principal criteria by which the quality of differential reflectivity estimates is evaluated. The paper is structured as follows. In section 2, a theoretical model is introduced along with the analysis of the cross-polar contaminant suppression mechanism. The ability of the QSHV mode to suppress cross-polar coupling terms and its sensitivity to reflectivity gradients are evaluated in section 3 using analytical derivations and simulated time series. Analysis where cross-polar coupling is emulated using time series collected with weather radar is given in section 4. The main conclusions of the paper are summarized in section 5.

2. Theoretical model

Cross-polarization coupling can be caused by precipitation or by the radar itself (e.g., as a result of the inherent cross-polarization fields generated by the antenna element and/or imperfections in the antenna, and by channel-to-channel cross coupling). Assuming a linear H, V polarization basis and no precipitation along the propagation path, the backscattering properties of a single noncanted hydrometeor can be described by its backscattering matrix $\mathbf{S}$, which relates the backscattered electric field vector $[\mathbf{E}]^b$ at the antenna to one $[\mathbf{E}]^i$ incident on the scatterer [Doviak and Zrnić 1993, Eq. (8.39)],

$$[\mathbf{E}]^b = \begin{bmatrix} E_h \\ E_v \end{bmatrix}^b = \begin{bmatrix} s_{hh} & s_{hv} \\ s_{vh} & s_{vv} \end{bmatrix} \begin{bmatrix} E_h \\ E_v \end{bmatrix}^i \frac{\exp(-jkr)}{r}, \quad (1)$$

where h and v denote the electric field's polarization, k is the precipitation-free wavenumber, and r is the distance from the radar to the scatterer.

The presence of distributed scatterers (e.g., precipitation) between the resolution volume and radar may alter the properties of the transmitted electric wave as it propagates (Oguchi 1983; Sachidananda and Zrnić 1985). Thus, $[\mathbf{E}]^i$ and $[\mathbf{E}]^b$ need to include the phase shifts and attenuation from the antenna ports to a far-field reference sphere incurred during propagation of the H and V fields through scattering media. This is known as the propagation effect and is usually quantified by the transmission matrix $\mathbf{T}$. Assuming there is no depolarization (i.e., hydrometeors have zero canting angle) nor differential attenuation at the 10-cm wavelengths of interest herein, the differential phase shift (ϕ_{DP}) is the dominant effect. Under these assumptions, $\mathbf{T}$ is (Doviak and Zrnić 1993)

$$\mathbf{T} = \begin{bmatrix} \exp(-j\phi_{DP}/2) & 0 \\ 0 & 1 \end{bmatrix}. \quad (2)$$

For weather radar application, the cross-polar radiation follows definition 2 given by Ludwig (1973). Excitation of the H port ideally generates purely horizontal (i.e.,$E_h \equiv E_v$) electric fields and excitation of the V port generates purely vertical (i.e., $E_v \equiv E_\theta$) electric fields. Terms E_θ and E_ϕ are electric field components in a spherical coordinate system with polar axis z vertical, and x is the direction broadside to the planar array—in this article the antenna is considered part of a planar polarimetric phased array radar (PPPAR). Angles θ and ϕ are the zenith and azimuth directions to the scatterer, respectively. In reality, however, excitation of the H or V ports always causes cross-polar fields having an intensity determined by the radiation matrix $\mathbf{F}$. It was analyzed by Zrnić et al. (2010) for a center-fed parabolic reflector antenna, who defined this matrix as

$$\mathbf{F} = \begin{bmatrix} F_{hh} & F_{hv} \\ F_{vh} & F_{vv} \end{bmatrix}, \quad (3)$$

where the matrix elements are one-way electric field patterns proportional to

$$F_{lp}(\theta_0, \theta; \phi_0, \phi) = |F_{lp}(\theta_0, \theta; \phi_0, \phi)| \exp[j\gamma_{lp}(\theta_0, \theta; \phi_0, \phi)]. \quad (4)$$

In (4), $j = \sqrt{-1}$, while indices l and p can either be h or v. Terms $F_{lp}(\theta_0, \theta; \phi_0, \phi)$ are complex radiation pattern functions that depend on beam direction θ_0, ϕ_0 in the case of phased array antennas but not in the case of parabolic reflectors. In both cases radiation pattern functions depend on the arguments θ, ϕ. The electric field patterns are characterized in the coordinate system that usually follows the Ludwig 2 or 3 definition with arguments θ, ϕ , where the boresight is at $\theta_0 = 0°$, $\phi_0 = 0°$.

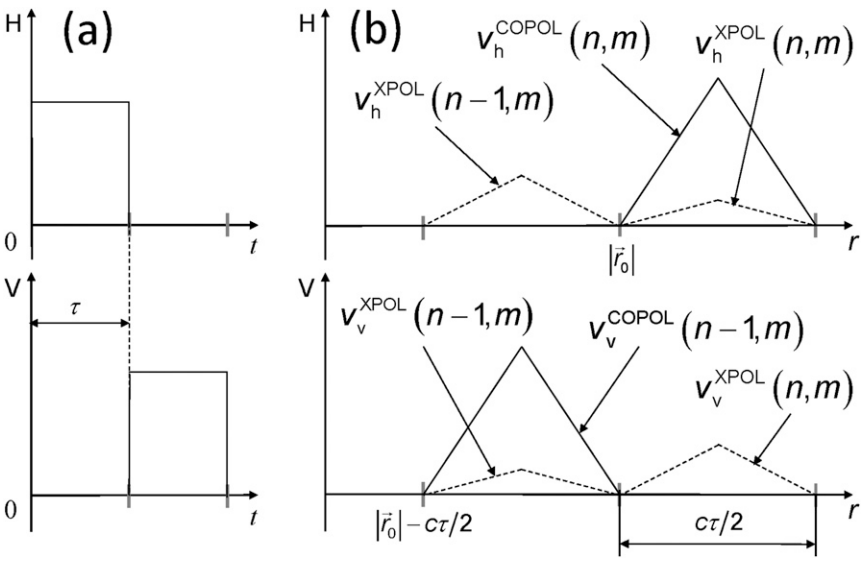

FIG. 1. (a) The time-muliplexing transmit scheme. (b) The copolar (solid) and cross-polar (dashed) received signal contributions from two adjacent resolution volumes V_6 uniformly filled with scatterers of the same properties. The signals arrive at the same time in each of the H and V receiving channels. The H and V samples to be simultaneously processed are one range gate apart (or τ in time), but the respective resolution volumes from copolar signals are aligned in range.

Term F_{hv} is the radiated H cross-polar electric field (i.e., cross-polar radiation pattern) if the V antenna port is excited, and vice versa for F_{vh}. In Zrnić et al. (2010), where cross coupling in parabolic antennas is investigated, F_{hh} and F_{vv} (i.e., copolar radiation patterns) are assumed to be real functions. However, for a PPPAR, F_{hh} and F_{vv} are complex—their amplitudes and phases vary for each beam position and are not equal (Zhang et al. 2009; Zrnić et al. 2011; Lei et al. 2015). Consequently, the differences between F_{hh} and F_{vv} introduce offsets in Z_{DR} and ϕ_{DP} estimates (i.e., copolar bias) that are dependent on boresight direction and must be accounted for (e.g., using calibration). Because all phases are considered relative to copolar H, F_{hh} is assumed to be real herein, and F_{vv} is complex. Also, F_{hv}, F_{vh} are assumed to encompass all hardware mechanisms, which contribute to cross coupling.

Further analysis is carried out assuming the following: 1) hydrometeors are oblate spheroids not canted, 2) amplitudes and phases of the transmitted H and V copolar radiation are not matched, and 3) differential attenuation along the path of propagation can, for most observations at 10-cm wavelengths, be neglected but the differential phase (ϕ_{DP}) cannot be neglected. Note that generally individual scatterers have canting angles that are not zero, but in most cases the mean canting angle of scatterers contained in a sufficiently large volume of space is zero. This provides a basis for the first assumption so that only depolarization incurred by the antenna cross-polar fields is considered herein (i.e., $s_{hv} = s_{vh} \approx 0$). The analysis presented here can be further expanded to include the presence of the depolarization and attenuation effects induced by scatterers and can be the topic for further research. We need not be specific about the multiple causes of channel-to-channel cross coupling, nor the causes of amplitude and phases of the radiation patterns F_{lp}. In case of PPPAR, the matrix **F** is different for each boresight direction so it accounts for the changes in the H and V channel electric field projections and changes in cross-polar fields as the beam is electronically steered in various directions [e.g., modeled by matrix **P** in Zhang et al. (2009) for a pair of crossed electric dipoles] and in channel-to-channel cross coupling.

As the transmitted pulses propagate through media, they illuminate scatterers and a portion of the energy is returned toward the radar. Herein, an ideal case is assumed where the transmitted pulses have constant phases, are rectangular in shape in both H and V, and are exactly one pulse width (τ) apart (Fig. 1a). If the H port is energized, then echo voltages $v_{hh}(\mathbf{r}_q, t, m)$ and $v_{vh}(\mathbf{r}_q, t, m)$ are received in H and V from the qth scatterer located in the direction θ, ϕ at range $\mathbf{r}_q$ and at time t (where $t = 2|\mathbf{r}_q|/c$ is the range–time measured from the start of the mth transmission and c is the speed of light). These are

$$\begin{bmatrix} v_{\rm hh}(\mathbf{r}_q,t,m) \\ v_{\rm vh}(\mathbf{r}_q,t,m) \end{bmatrix} = C\mathbf{F}^{\rm T}\mathbf{T}^{\rm T}\mathbf{STFE}_{\rm P},$$

$$= C\begin{bmatrix} F_{\rm hh} & F_{\rm vh} \\ F_{\rm hv} & F_{\rm vv} \end{bmatrix}\begin{bmatrix} s'_{\rm hh}(q) & 0 \\ 0 & s_{\rm vv}(q) \end{bmatrix}\begin{bmatrix} F_{\rm hh} & F_{\rm hv} \\ F_{\rm vh} & F_{\rm vv} \end{bmatrix}\begin{bmatrix} p\left(t+\tau-2\dfrac{|\mathbf{r}_q|}{c}\right) \\ 0 \end{bmatrix} e^{-j2kr_q(m)}, \tag{5a}$$

where superscript T indicates the transposed matrix, $s'_{\rm hh}(n) \equiv s_{\rm hh}(n)e^{-j\phi_{\rm DP}}$, arguments of F_{lp} are not explicitly shown, and C is a scalar factor that contains a dependence on range $\mathbf{r}_0$ to resolution volume V_6 [i.e., volume encompassed by the radar beam illuminating scatterers of interest (Doviak and Zrnić 1993)], attenuation, and system parameters. The second subscript in F_{lp} indicates the energized (transmitting) port and the first subscript is the receiving port. The symbol p denotes the transmitted pulse shapes, which are assumed to be the same in both H and V.

If V port is energized immediately after H port, the echo voltages $v_{\rm vv}(\mathbf{r}_i, t, m)$ and $v_{\rm hv}(\mathbf{r}_i, t, m)$ are received at time t in V and H from the ith scatterer located at range $\mathbf{r}_i$ (where $|\mathbf{r}_i| = |\mathbf{r}_q| - c\tau/2$). These are

$$\begin{bmatrix} v_{\rm hv}(\mathbf{r}_i,t,m) \\ v_{\rm vv}(\mathbf{r}_i,t,m) \end{bmatrix} = C\mathbf{F}^{\rm T}\mathbf{T}^{\rm T}\mathbf{STFE}_{P}$$

$$= \begin{bmatrix} F_{\rm hh} & F_{\rm vh} \\ F_{\rm hv} & F_{\rm vv} \end{bmatrix}\begin{bmatrix} s'_{\rm hh}(i) & 0 \\ 0 & s_{\rm vv}(i) \end{bmatrix}\begin{bmatrix} F_{\rm hh} & F_{\rm hv} \\ F_{\rm vh} & F_{\rm vv} \end{bmatrix}\begin{bmatrix} 0 \\ p\left(t-2\dfrac{|\mathbf{r}_i|}{c}\right)e^{j\beta} \end{bmatrix} e^{-j2kr_i(m)}, \tag{5b}$$

where the symbol β denotes the phase difference between H and V imposed on transmission. Carrying out the matrix multiplication, the two scatterers create composite H and V echo voltages at time t as

$$\begin{aligned} v_{\rm h}(\mathbf{r}_q,t,m) &= v_{\rm hh}(\mathbf{r}_q,t,m) + v_{\rm hv}(\mathbf{r}_i,t,m), \\ &= C\left\{[F_{\rm hh}^2 s'_{\rm hh}(q) + F_{\rm vh}^2 s_{\rm vv}(q)]p\left(t+\tau-2\frac{|\mathbf{r}_q|}{c}\right)e^{-j2kr_q(m)}\right. \\ &\quad \left. + [F_{\rm hh}F_{\rm hv}s'_{\rm hh}(i) + F_{\rm vv}F_{\rm vh}s_{\rm vv}(i)]p\left(t-2\frac{|\mathbf{r}_i|}{c}\right)e^{j[\beta-2kr_i(m)]}\right\}. \\ v_{\rm v}(\mathbf{r}_i,t,m) &= v_{\rm vv}(\mathbf{r}_i,t,m) + v_{\rm vh}(\mathbf{r}_q,t,m), \\ &= C\left\{[F_{\rm hv}^2 s'_{\rm hh}(i) + F_{\rm vv}^2 s_{\rm vv}(i)]p\left(t-2\frac{|\mathbf{r}_i|}{c}\right)e^{j[\beta-2kr_i(m)]}\right. \\ &\quad \left. + [F_{\rm hh}F_{\rm hv}s'_{\rm hh}(q) + F_{\rm vv}F_{\rm vh}s_{\rm vv}(q)]p\left(t+\tau-2\frac{|\mathbf{r}_q|}{c}\right)e^{-j2kr_q(m)}\right\}. \end{aligned} \tag{6}$$

For simplicity the effects of the phase difference as a result of signal propagation through the H and V receiver paths are neglected as they have no bearing on the results reported herein.

The echo voltages from scatterers in the resolution volume V_6 at $\mathbf{r}_0$ (covering the range between $|\mathbf{r}_0|$ and $|\mathbf{r}_0| + c\tau/2$) can be viewed as the sums of incremental voltages caused by scatterers in infinitely thin subvolumes dV_6 at $\mathbf{r}$ (i.e., $|\mathbf{r}_0| \le |\mathbf{r}| \le |\mathbf{r}_0| + c\tau/2$). If subvolumes dV_6 are sufficiently small in azimuth and elevation compared to the changes in antenna radiation patterns, then F_{lp} can be considered practically constant over each dV_6. Then, the incremental voltage from scatterers in dV_6 is

$$dv_l(\mathbf{r}_d,t,m) = \sum_d v_l(\mathbf{r}_d,t,m), \tag{7}$$

where l is h or v and d is q or i. The substitution of (6) into (7) yields

$$dv_{\mathrm{h}}(\mathbf{r}_q,t,m)=C\Bigg\{\sum_q[F_{\mathrm{hh}}^2 s'_{\mathrm{hh}}(q)+F_{\mathrm{vh}}^2 s_{\mathrm{vv}}(q)]p\left(t+\tau-2\frac{|\mathbf{r}_q|}{c}\right)e^{-j2kr_q(m)}$$
$$+\sum_i[F_{\mathrm{hh}}F_{\mathrm{hv}}s'_{\mathrm{hh}}(i)+F_{\mathrm{vv}}F_{\mathrm{vh}}s_{\mathrm{vv}}(i)]p\left(t-2\frac{|\mathbf{r}_i|}{c}\right)e^{j[\beta-2kr_i(m)]}\Bigg\}.$$
$$dv_{\mathrm{v}}(\mathbf{r}_i,t,m)=C\Bigg\{\sum_i[F_{\mathrm{hv}}^2 s'_{\mathrm{hh}}(i)+F_{\mathrm{vv}}^2 s_{\mathrm{vv}}(i)]p\left(t-2\frac{|\mathbf{r}_i|}{c}\right)e^{j[\beta-2kr_i(m)]}$$
$$+\sum_q[F_{\mathrm{hh}}F_{\mathrm{hv}}s'_{\mathrm{hh}}(q)+F_{\mathrm{vv}}F_{\mathrm{vh}}s_{\mathrm{vv}}(q)]p\left(t+\tau-2\frac{|\mathbf{r}_q|}{c}\right)e^{-j2kr_q(m)}\Bigg\}. \tag{8}$$

Assuming scatterers of various equivalent volume diameters are uniformly distributed within dV_6, an incremental scattering matrix $\mathbf{S}$, for each dV_6, can be defined having elements on the main diagonal,

$$s'_{\mathrm{hh}}(|\mathbf{r}_q|,m)=\sum_q Cs'_{\mathrm{hh}}(q)e^{-j2kr_q(m)};$$
$$s'_{\mathrm{hh}}\left(|\mathbf{r}_q|-c\tau/2,m\right)=\sum_i Cs'_{\mathrm{hh}}(i)e^{-j2kr_i(m)},$$
$$s_{\mathrm{vv}}(|\mathbf{r}_q|,m)=\sum_q Cs_{\mathrm{vv}}(q)e^{-j2kr_q(m)};$$
$$s_{\mathrm{vv}}\left(|\mathbf{r}_q|-c\tau/2,m\right)=\sum_i Cs_{\mathrm{vv}}(i)e^{-j2kr_i(m)}. \tag{9}$$

Because elements of $\mathbf{S}$ account for the fact that scatterers within dV_6 have different relative ranges for every m, they have random real and imaginary parts that are zero mean and Gaussian distributed functions of m, unlike the unchanging scattering matrix of a single scatterer not wobbling nor oscillating. Note that the dependence of $s'_{\mathrm{hh}}(|\mathbf{r}_q|, m)$ and $s_{\mathrm{vv}}(|\mathbf{r}_q|, m)$ on m is clearly stated, which differentiates these from the elements of a single scatterer scattering matrix $\mathbf{S}$. Hence, each V_6 at range $\mathbf{r}_0$ consists of subvolumes dV_6, covers an area of approximately $|\mathbf{r}_0|$ to $|\mathbf{r}_0|+c\tau/2$ in range, and is bounded by the span of copolar and cross-polar antenna patterns in azimuth and elevation. Voltages received at time t in the H and V receivers are

$$v_{\mathrm{h}}(t,m)=\int_\Omega\Bigg\{\int_{ct/2}^{ct/2+c\tau/2}[F_{\mathrm{hh}}^2 s'_{\mathrm{hh}}(r,m)+F_{\mathrm{vh}}^2 s_{\mathrm{vv}}(r,m)]p\left(t+\tau-2\frac{r}{c}\right)dr$$
$$+e^{j\beta}\int_{ct/2-c\tau/2}^{ct/2}[F_{\mathrm{hh}}F_{\mathrm{hv}}s'_{\mathrm{hh}}(r,m)+F_{\mathrm{vv}}F_{\mathrm{vh}}s_{\mathrm{vv}}(r,m)]p\left(t-2\frac{r}{c}\right)dr\Bigg\}d\Omega.$$
$$v_{\mathrm{v}}(t,m)=\int_\Omega\Bigg\{e^{j\beta}\int_{ct/2-c\tau/2}^{ct/2}[F_{\mathrm{vv}}^2 s_{\mathrm{vv}}(r,m)+F_{\mathrm{hv}}^2 s'_{\mathrm{hh}}(r,m)]p\left(t-2\frac{r}{c}\right)dr$$
$$+\int_{ct/2}^{ct/2+c\tau/2}[F_{\mathrm{hh}}F_{\mathrm{hv}}s'_{\mathrm{hh}}(r,m)+F_{\mathrm{vv}}F_{\mathrm{vh}}s_{\mathrm{vv}}(r,m)]p\left(t+\tau-2\frac{r}{c}\right)dr\Bigg\}d\Omega. \tag{10}$$

In (10) the integral over θ and ϕ is replaced with the integral over the solid angle Ω so that $d\Omega\equiv\sin(\theta)d\theta d\phi$. Also, a large signal-to-noise ratio (SNR) is assumed so that the influence of noise can be neglected.

If echo voltages $v_{\mathrm{h}}(t, m)$ and $v_{\mathrm{v}}(t, m)$ are sampled at discrete intervals $n\tau$ their sampled values in H and V are

$$V_{\mathrm{h}}(n,m)=\int_\Omega[v_{\mathrm{h}}^{\mathrm{COPOL}}(n,m)+v_{\mathrm{h}}^{\mathrm{XPOL}}(n,m)+v_{\mathrm{h}}^{\mathrm{XPOL}}(n-1,m)]\,d\Omega$$
$$V_{\mathrm{v}}(n,m)=\int_\Omega[v_{\mathrm{v}}^{\mathrm{COPOL}}(n-1,m)+v_{\mathrm{v}}^{\mathrm{XPOL}}(n-1,m)+v_{\mathrm{v}}^{\mathrm{XPOL}}(n,m)]\,d\Omega, \tag{11}$$

where

$$
\begin{aligned}
v_{\mathrm{h}}^{\mathrm{COPOL}}(n,m) &= F_{\mathrm{hh}}^2 s'_{\mathrm{hh}}(n,m),\\
v_{\mathrm{h}}^{\mathrm{XPOL}}(n,m) &= F_{\mathrm{vh}}^2 s_{\mathrm{vv}}(n,m),\\
v_{\mathrm{h}}^{\mathrm{COPOL}}(n-1,m) &= e^{j\beta}[F_{\mathrm{hh}}F_{\mathrm{hv}}s'_{\mathrm{hh}}(n-1,m) + F_{\mathrm{vv}}F_{\mathrm{vh}}s_{\mathrm{vv}}(n-1,m)],\\
v_{\mathrm{v}}^{\mathrm{COPOL}}(n-1,m) &= e^{j\beta}F_{\mathrm{vv}}^2 s_{\mathrm{vv}}(n-1,m),\\
v_{\mathrm{v}}^{\mathrm{XPOL}}(n-1,m) &= e^{j\beta}F_{\mathrm{hv}}^2 s'_{\mathrm{hh}}(n-1,m),\\
v_{\mathrm{v}}^{\mathrm{COPOL}}(n,m) &= [F_{\mathrm{hh}}F_{\mathrm{hv}}s'_{\mathrm{hh}}(n,m) + F_{\mathrm{vv}}F_{\mathrm{vh}}s_{\mathrm{vv}}(n,m)],
\end{aligned}
\tag{12}
$$

and

$$
\begin{aligned}
s'_{\mathrm{hh}}(n,m) &= \int_{nc\tau/2}^{(n+1)c\tau/2} s'_{\mathrm{hh}}(r,m)p\left(n\frac{c\tau}{2}+\tau-2\frac{r}{c}\right)dr,\\
s_{\mathrm{vv}}(n,m) &= \int_{nc\tau/2}^{(n+1)c\tau/2} s_{\mathrm{vv}}(r,m)p\left(n\frac{c\tau}{2}+\tau-2\frac{r}{c}\right)dr,\\
s'_{\mathrm{hh}}(n-1,m) &= \int_{(n-1)c\tau/2}^{nc\tau/2} s'_{\mathrm{hh}}(r,m)p\left(n\frac{c\tau}{2}-2\frac{r}{c}\right)dr,\\
s_{\mathrm{vv}}(n-1,m) &= \int_{(n-1)c\tau/2}^{nc\tau/2} s_{\mathrm{vv}}(r,m)p\left(n\frac{c\tau}{2}-2\frac{r}{c}\right)dr.
\end{aligned}
\tag{13}
$$

In (11)–(13) n designates the range bin number (corresponding to V_6 located at range $nc\tau/2$) counted from the start of the H pulse transmission.

Expression (11) shows that samples taken at times $n\tau + mT_s$ (where T_s is the pulse repetition time) are sums of echoes from scatterers that cover the range of two pulse widths (i.e., $c\tau$), where the resolution volumes of copolar returns in H and V are shifted by $c\tau/2$, in range with respect to each other as shown in Fig. 1b. To align the V_6 from the respective copolar returns, samples taken at $n\tau + mT_s$ in H and those taken at $(n+1)\tau + mT_s$ in V ought to be combined when computing the polarimetric variables. In general, if the time interval between consecutive samples is τ, then the delay between the transmission of H and V pulses should be an integer multiple of τ. Then, if the V field is radiated $K\tau$ seconds after H field (or vice versa), the respective copolar returns can always be aligned by combining samples, from the H and V channels, that are $K\tau$ seconds apart. In such a case, care should be taken so that the delay $K\tau$ does not incur appreciable decorrelation of the aligned samples from the two channels. Herein, a case where $K = 1$ is considered so the aligned sampled voltages from the mth transmission are

$$
\begin{aligned}
V_{\mathrm{h}}(n,m) &\sim \int_{\Omega}\{F_{\mathrm{hh}}^2 s'_{\mathrm{hh}}(n,m) + F_{\mathrm{vh}}^2 s_{\mathrm{vv}}(n,m) + [F_{\mathrm{hh}}F_{\mathrm{hv}}s'_{\mathrm{hh}}(n-1,m) + F_{\mathrm{vv}}F_{\mathrm{vh}}s_{\mathrm{vv}}(n-1,m)]e^{j\beta}\}\,d\Omega,\\
V_{\mathrm{v}}(n+1,m) &\sim \int_{\Omega}\{[F_{\mathrm{hv}}^2 s'_{\mathrm{hh}}(n,m) + F_{\mathrm{vv}}^2 s_{\mathrm{vv}}(n,m)]e^{j\beta} + [F_{\mathrm{hh}}F_{\mathrm{hv}}s'_{\mathrm{hh}}(n+1,m) + F_{\mathrm{vv}}F_{\mathrm{vh}}s_{\mathrm{vv}}(n+1,m)]\}\,d\Omega.
\end{aligned}
\tag{14}
$$

The powers now become

$$
\begin{aligned}
P_{\mathrm{h}}(n,m) &= |V_{\mathrm{h}}(n,m)|^2 \approx \int_{\Omega}[F_{\mathrm{hh}}^4|s_{\mathrm{hh}}(n,m)|^2 + \delta P_{1\mathrm{h}}(n,m) + \delta P_{2\mathrm{h}}(n,m)]\,d\Omega,\\
P_{\mathrm{v}}(n+1,m) &= |V_{\mathrm{v}}(n+1,m)|^2 \approx \int_{\Omega}[|F_{\mathrm{vv}}|^2|s_{\mathrm{vv}}(n,m)|^2 + \delta P_{1\mathrm{v}}(n+1,m) + \delta P_{2\mathrm{v}}(n+1,m)]\,d\Omega,
\end{aligned}
\tag{15}
$$

where

$$\begin{aligned}
\delta P_{1h}(n,m) &= F_{hh}^2|F_{hv}|^2|s'_{hh}(n-1,m)|^2 + |F_{vv}|^2|F_{vh}|^2|s_{vv}(n-1,m)|^2 \\
&\quad + 2\mathrm{Re}[F_{hh}^2F_{vh}^2s'^*_{hh}(n,m)s_{vv}(n,m) + F_{hh}F_{vv}F^*_{hv}F_{vh}s'^*_{hh}(n-1,m)s_{vv}(n-1,m)], \\
\delta P_{2h}(n,m) &= 2\mathrm{Re}\{[F_{hh}^3F_{hv}s'^*_{hh}(n,m)s'_{hh}(n-1,m) + F_{hh}^2F_{vv}F_{vh}s'^*_{hh}(n,m)s_{vv}(n-1,m)]e^{j\beta}\}, \\
\delta P_{1v}(n+1,m) &= |F_{vv}|^2|F_{vh}|^2|s_{vv}(n+1,m)|^2 + F_{hh}^2|F_{hv}|^2|s'_{hh}(n+1,m)|^2 \\
&\quad + 2\mathrm{Re}[(F^*_{vv})^2F_{hv}^2s^*_{vv}(n,m)s'_{hh}(n,m) + F_{hh}F^*_{vv}F^*_{vh}F_{hv}s^*_{vv}(n+1,m)s'_{hh}(n+1,m)], \\
\delta P_{2v}(n+1,m) &= 2\mathrm{Re}\{[|F_{vv}|^2F^*_{vv}F_{vh}s^*_{vv}(n,m)s_{vv}(n+1,m) + (F^*_{vv})^2F_{hh}F_{hv}s^*_{vv}(n,m)s'_{hh}(n+1,m)]e^{-j\beta}\}
\end{aligned} \tag{16}$$

are the bias terms in the powers measured in H and V. Note that all products in which F_{hh} or F_{vv} appear only once are discarded because these do not add appreciably to the total power.

3. Cross-polar isolation quality assessment

In this work the bias and standard deviation are the principal criteria by which the quality of differential reflectivity estimates are evaluated. Bias smaller than 0.1 dB for $Z_{DR}\in(0, 1]$ or smaller than 0.1 Z_{DR} at $Z_{DR} >$ 1 dB is deemed satisfactory (Zrnić et al. 2010). For simplicity, the distribution of scatterers within the resolution volume is assumed homogeneous for radar with narrow beam. Thus, $\langle s_{ll}(n, m)\rangle$ is not a function of Ω in the analysis presented herein.

Because the array factor for large PPPAR antennas is a highly peaked function of θ, ϕ relative to the smooth changes of the element patterns (Balanis 2005, section 6.10.1), it is likely H and V copolar pattern shapes will be well matched for beam directions of interest. Sufficient matching of the H and V copolar radiation patterns in shape is also the principal assumption of dual polarimetry so that these do not introduce appreciable biases in polarimetric variable estimates. Thus, $|F_{hh}| \approx |F_{vv}|$ is assumed herein. However, it is almost certain that the amplitude and phase of the copolar beams will differ and vary with beam direction (Bhardwaj and Rahmat-Samii 2014; Lei et al. 2015). For simplicity it is assumed that phases are constant across the main beam from which most echo power is received.

For a center-fed parabolic reflector, the cross-polar pattern has four equal amplitude major lobes with a null along the copolar beam axis (Jones 1954; Zrnić et al. 2010). Such cross-polar patterns create less bias than if copolar and cross-polar beams are coaxial. However, for PPPAR, copolar and cross-polar beams are coaxial if beams are directed away from the principal planes (Lei et al. 2015). For the purpose of analysis herein, the worst case is assumed where copolar and cross-polar beams are coaxial and have the same shape. Thus, fields across the copolar and cross-polar beams can only differ in peak amplitude and phase, which is the case analyzed here. In realistic design, however, it is likely that the sidelobes of copolar and cross-polar patterns will not have the same shapes (Perera et al. 2013). But if sidelobes of copolar and cross-polar patterns are small with respect to the main lobes, then the main beams of the copolar and cross-polar patterns will have the most impact on the bias of polarimetric variable estimates. Given that copolar and cross-polar radiation patterns have the same shape, they can be represented as

$$\begin{aligned}
F_{lp}(\theta_0,\theta;\phi_0,\phi) &= \sqrt{g_{lp}(\theta_0,\phi_0)}f(\theta_0,\theta;\phi_0,\phi) \\
&\quad \times \exp[j\gamma_{lp}(\theta_0,\theta;\phi_0,\phi)],
\end{aligned} \tag{17}$$

where l and p can either be h or v. A normalization can be applied so that

$$\int_\Omega |f(\theta_0,\theta;\phi_0,\phi)|^4\, d\Omega = 1. \tag{18}$$

Then $g_{lp}(\theta_0, \phi_0)$ is an integrated real number that describes the dependence of the antenna pattern on a boresight direction. Given the assumption that all radiation patterns are the same in shape, but copolar and cross-polar H and V patterns differ in magnitude and phase, the effectiveness of the cross-polar fields in creating Z_{DR} bias can be expressed in terms of a cross-polar coupling factor cpcf (or CPCF in decibels), defined as

$$\begin{aligned}
\mathrm{cpcf}_h(\theta_0,\phi_0) &= \frac{\int_\Omega F_{hh}^2|F_{hv}|^2\, d\Omega}{\int_\Omega F_{hh}^4\, d\Omega} = \frac{g_{hv}(\theta_0,\phi_0)}{g_{hh}(\theta_0,\phi_0)}; \\
\mathrm{CPCF}_h(\theta_0,\phi_0) &= 10\log_{10}[\mathrm{cpcf}_h(\theta_0,\phi_0)], \\
\mathrm{cpcf}_v(\theta_0,\phi_0) &= \frac{\int_\Omega |F_{vv}|^2|F_{vh}|^2\, d\Omega}{\int_\Omega |F_{vv}|^4\, d\Omega} = \frac{g_{vh}(\theta_0,\phi_0)}{g_{vv}(\theta_0,\phi_0)}; \\
\mathrm{CPCF}_v(\theta_0,\phi_0) &= 10\log_{10}[\mathrm{cpcf}_v(\theta_0,\phi_0)].
\end{aligned} \tag{19}$$

Thus, $\mathrm{cpcf}_h(\theta_0, \phi_0)$ is the ratio of the peak power in the V cross-polar pattern (i.e., the power at boresight)

to the peak power in the H copolar pattern and vice versa for $\mathrm{cpcf_v}(\theta_0, \phi_0)$. Under the stipulated assumptions, the cross-polar radiation terms can be represented as

$$F_{\mathrm{vh}}(\theta_0, \theta; \phi_0, \phi) = \sqrt{g_{\mathrm{vv}}(\theta_0, \phi_0)\mathrm{cpcf_v}(\theta_0, \phi_0)} f(\theta_0, \theta; \phi_0, \phi) \exp[j\gamma_{\mathrm{vh}}(\theta_0, \theta; \phi_0, \phi)],$$
$$F_{\mathrm{hv}}(\theta_0, \theta; \phi_0, \phi) = \sqrt{g_{\mathrm{hh}}(\theta_0, \phi_0)\mathrm{cpcf_h}(\theta_0, \phi_0)} f(\theta_0, \theta; \phi_0, \phi) \exp[j\gamma_{\mathrm{hv}}(\theta_0, \theta; \phi_0, \phi)]. \quad (20)$$

Because $\langle s_{ll}(n, m)\rangle$ is not a function of Ω, it can be placed in front of the integration symbol in (15) to obtain the mean values as

$$\begin{aligned}\langle P_{\mathrm{h}}(n,m)\rangle &= \left\langle \int_\Omega [F_{\mathrm{hh}}^4 |s'_{\mathrm{hh}}(n,m)|^2 + \delta P_{1\mathrm{h}}(n,m) + \delta P_{2\mathrm{h}}(n,m)]\, d\Omega \right\rangle \\ &= g_{\mathrm{hh}}^2 \langle |s'_{\mathrm{hh}}(n,m)|^2\rangle + \left\langle \int_\Omega \delta P_{1\mathrm{h}}(n,m)\, d\Omega \right\rangle \\ \langle P_{\mathrm{v}}(n+1,m)\rangle &= \left\langle \int_\Omega [|F_{\mathrm{vv}}|^4 |s_{\mathrm{vv}}(n,m)|^2 + \delta P_{1\mathrm{v}}(n+1,m) + \delta P_{2\mathrm{v}}(n+1,m)]\, d\Omega \right\rangle \\ &= g_{\mathrm{vv}}^2 \langle |s_{\mathrm{vv}}(n,m)|^2\rangle + \left\langle \int_\Omega \delta P_{1\mathrm{v}}(n+1,m)\, d\Omega \right\rangle, \end{aligned} \quad (21)$$

where the bias in H power is

$$\begin{aligned}\left\langle \int_\Omega \delta P_{1\mathrm{h}}(n,m)\, d\Omega \right\rangle &= g_{\mathrm{hh}}^2 \mathrm{cpcf_h} \langle |s_{\mathrm{hh}}(n-1,m)|^2\rangle + g_{\mathrm{vv}}^2 \mathrm{cpcf_v} \langle |s_{\mathrm{vv}}(n-1,m)|^2\rangle \\ &\quad + 2g_{\mathrm{hh}} g_{\mathrm{vv}} \mathrm{Re}[\mathrm{cpcf_v} e^{j2\gamma_{\mathrm{vh}}} \langle s_{\mathrm{hh}}^*(n,m) s_{\mathrm{vv}}(n,m)\rangle \\ &\quad + \sqrt{\mathrm{cpcf_h}\mathrm{cpcf_v}}\, e^{j(\gamma_{\mathrm{vv}}+\gamma_{\mathrm{vh}}-\gamma_{\mathrm{hv}})} \langle s_{\mathrm{hh}}^*(n-1,m) s_{\mathrm{vv}}(n-1,m)\rangle], \end{aligned} \quad (22a)$$

$$\begin{aligned}\left\langle \int_\Omega \delta P_{2\mathrm{h}}(n,m)\, d\Omega \right\rangle &= 2\mathrm{Re}[g_{\mathrm{hh}}^2 \sqrt{\mathrm{cpcf_h}}\, e^{j(\gamma_{\mathrm{hv}}+\beta)} \langle s_{\mathrm{hh}}^*(n,m) s_{\mathrm{hh}}(n-1,m)\rangle \\ &\quad + g_{\mathrm{hh}} g_{\mathrm{vv}} \sqrt{\mathrm{cpcf_v}}\, e^{j(\gamma_{\mathrm{vv}}+\gamma_{\mathrm{vh}}+\beta)} \langle s_{\mathrm{hh}}^*(n,m) s_{\mathrm{vv}}(n-1,m)\rangle], \\ &= 0, \end{aligned} \quad (22b)$$

and in V

$$\begin{aligned}\left\langle \int_\Omega \delta P_{1\mathrm{v}}(n+1,m)\, d\Omega \right\rangle &= g_{\mathrm{vv}}^2 \mathrm{cpcf_v} \langle |s_{\mathrm{vv}}(n+1,m)|^2\rangle + g_{\mathrm{hh}}^2 \mathrm{cpcf_h} \langle |s_{\mathrm{hh}}(n+1,m)|^2\rangle \\ &\quad + 2g_{\mathrm{hh}} g_{\mathrm{vv}} \mathrm{Re}[\mathrm{cpcf_h} e^{j2(\gamma_{\mathrm{hv}}-\gamma_{\mathrm{vv}})} \langle s_{\mathrm{vv}}^*(n,m) s_{\mathrm{hh}}(n,m)\rangle \\ &\quad + \sqrt{\mathrm{cpcf_h}\mathrm{cpcf_v}}\, e^{j(\gamma_{\mathrm{hv}}-\gamma_{\mathrm{vh}}-\gamma_{\mathrm{vv}})} \langle s_{\mathrm{vv}}^*(n+1,m) s_{\mathrm{hh}}(n+1,m)\rangle], \end{aligned} \quad (23a)$$

$$\begin{aligned}\left\langle \int_\Omega \delta P_{2\mathrm{v}}(n+1,m)\, d\Omega \right\rangle &= 2\mathrm{Re}[g_{\mathrm{vv}}^2 \sqrt{\mathrm{cpcf_v}}\, e^{j(\gamma_{\mathrm{vh}}-\gamma_{\mathrm{vv}}-\beta)} \langle s_{\mathrm{vv}}^*(n,m) s_{\mathrm{vv}}(n+1,m)\rangle \\ &\quad + g_{\mathrm{hh}} g_{\mathrm{vv}} \sqrt{\mathrm{cpcf_h}}\, e^{j(\gamma_{\mathrm{hv}}-2\gamma_{\mathrm{vv}}-\beta)} \langle s_{\mathrm{vv}}^*(n,m) s_{\mathrm{hh}}(n+1,m)\rangle] \\ &= 0. \end{aligned} \quad (23b)$$

Note that because the returns from adjacent resolution volumes are considered uncorrelated, the mean values of (22b) and (23b) are zero and are therefore omitted from (21).

Furthermore, because $s'_{\mathrm{hh}}(n, m)$ and $s_{\mathrm{vv}}(n, m)$ describe the ensemble of scatterers contained within V_6, these can be generated using Monte Carlo simulations as described in Zrnić (1975) and Galati and Pavan (1995).

Because the cited articles assume copolar beams having gain independent of boresight direction, and no cross-coupling, these voltage samples, simulated for every dV_6, can be used in place of $s'_{hh}(m)$ and $s_{vv}(m)$ in (14) to obtain $V_l(n, m)$. Consequently, constructed samples account for the effects of cross coupling as well as QSHV mode of operation. Hence, with the spatial integration of the incremental contributions, this approach (or model) allows for analysis of Z_{DR} bias and standard deviation using simulated time series and also provides for investigation of the effects that nonuniformities in the properties of scatterers across V_6 have on radar products. Furthermore, simulated and measured F_{lp} can be used to produce realistic weather echo voltages that can be used to assess polarimetric radar performance (Chandrasekar and Keeler 1993).

A differential reflectivity is computed as

$$\hat{Z}_{DR} = 10\log_{10}\left(\frac{\hat{S}_h^{NX} + \delta\hat{P}_h}{\hat{S}_v^{NX} + \delta\hat{P}_v}\right), \tag{24}$$

where the superscript NX denotes the estimates unbiased by the cross coupling (i.e., $F_{hv} = F_{vh} = 0$) and

$$\hat{S}_h^{NX} = \frac{1}{M}\sum_{m=0}^{M-1}\left|\int_\Omega F_{hh}^2 s'_{hh}(n,m)\,d\Omega + n_h(n,m)\right|^2 - N_h$$

$$\hat{S}_v^{NX} = \frac{1}{M}\sum_{m=0}^{M-1}\left|\int_\Omega F_{vv}^2 s_{vv}(n,m)\,d\Omega + n_v(n,m)\right|^2 - N_v$$

$$\delta\hat{P}_h = \frac{1}{M}\sum_{m=0}^{M-1}\int_\Omega [\delta P_{1h}(n,m) + \delta P_{2h}(n,m)]\,d\Omega$$

$$\delta\hat{P}_v = \frac{1}{M}\sum_{m=0}^{M-1}\int_\Omega [\delta P_{1v}(n+1,m) + \delta P_{2v}(n+1,m)]\,d\Omega, \tag{25}$$

where $n_h(n, m)$ and $n_v(n, m)$ are the mth samples of noise voltage, while $N_h = \langle|n_h(n,m)|^2\rangle$ and $N_v = \langle|n_v(n,m)|^2\rangle$ are the mean noise powers in the H and V channels, respectively. After expanding (24) into Taylor series of the first order, it becomes

$$\hat{Z}_{DR} \approx \hat{Z}_{DR}^{NX} + \frac{10}{\ln(10)}\left(\frac{\delta\hat{P}_h}{\hat{S}_h^{NX}} - \frac{\delta\hat{P}_v}{\hat{S}_v^{NX}}\right), \tag{26}$$

where $\hat{Z}_{DR}^{NX}$ is the M-sample average estimate if cross coupling is zero (i.e., $\hat{Z}_{DR}^{NX} = 10\log_{10}(\hat{S}_h^{NX}/\hat{S}_v^{NX})$), and generally $g_{hh} \neq g_{vv}$ (note that the dependency of g_{lp} on θ_0, ϕ_0 is implicit herein as is later in the text). Because g_{hh} and g_{vv} of a PPPAR have different dependencies on boresight direction, $\hat{Z}_{DR}^{NX}$ is a biased estimate of Z_{DR} in which the bias is a function of boresight direction but independent of the scatterers' properties. Thus, the PPPAR will need to be calibrated for each beam position to account for this component of Z_{DR} estimate bias [i.e., copolar Z_{DR} bias; $\text{BIAS}_{co}(\hat{Z}_{DR}) = Z_{DR} - \langle\hat{Z}_{DR}^{NX}\rangle = 10\log_{10}(g_{hh}^2/g_{vv}^2)$]. Then, the second term in (26) is the bias component induced solely by cross coupling and its expected value $\text{BIAS}_X(\hat{Z}_{DR})$ (X in the subscript denotes cross coupling) is

$$\begin{aligned}
\langle\text{BIAS}_X(\hat{Z}_{DR})\rangle &= \langle\hat{Z}_{DR}\rangle - \langle\hat{Z}_{DR}^{NX}\rangle \\
&\approx \frac{10}{\ln(10)}\frac{\langle\delta\hat{P}_h\rangle}{\langle\hat{S}_h^{NX}\rangle} - \frac{10}{\ln(10)}\frac{\langle\delta\hat{P}_v\rangle}{\langle\hat{S}_v^{NX}\rangle} \\
&\approx \frac{10}{\ln(10)}\left\{\frac{S_h(n-1)}{S_h(n)}\left[\text{cpcf}_h + \frac{g_{vv}^2}{g_{hh}^2}\text{cpcf}_v Z_{dr}^{-1}(n-1)\right]\right. \\
&\quad - \frac{S_v(n+1)}{S_v(n)}\left[\text{cpcf}_v + \frac{g_{hh}^2}{g_{vv}^2}\text{cpcf}_h Z_{dr}(n+1)\right] \\
&\quad + 2|\rho_{hv}(n,0)|\times\left[\frac{g_{vv}}{g_{hh}}\text{cpcf}_v\sqrt{Z_{dr}^{-1}(n)}\cos[2\gamma_{vh} + \phi_{DP}(n)]\right. \\
&\quad \left.\left. - \frac{g_{hh}}{g_{vv}}\text{cpcf}_h\sqrt{Z_{dr}(n)}\cos[2\gamma_{hv} - 2\gamma_{vv} - \phi_{DP}(n)]\right] + 2\sqrt{\text{cpcf}_h\text{cpcf}_v}\right. \\
&\quad \times\left[\frac{g_{vv}}{g_{hh}}|\rho_{hv}(n-1,0)|\frac{\sqrt{S_h(n-1)S_v(n-1)}}{S_h(n)}\cos[\gamma_{vh} - \gamma_{hv} + \gamma_{vv} + \phi_{DP}(n-1)]\right. \\
&\quad \left.\left. - \frac{g_{hh}}{g_{vv}}|\rho_{hv}(n+1,0)|\frac{\sqrt{S_h(n+1)S_v(n+1)}}{S_v(n)}\cos[\gamma_{hv} - \gamma_{vh} - \gamma_{vv} - \phi_{DP}(n+1)]\right\}(\text{dB}),
\end{aligned} \tag{27}$$

where $S_h(n)$, $S_v(n)$ and Z_{dr} are

$$S_h(n) = \frac{1}{M}\sum_{m=0}^{M-1}\langle|s_{hh}(n,m)|^2\rangle$$
$$S_v(n) = \frac{1}{M}\sum_{m=0}^{M-1}\langle|s_{vv}(n,m)|^2\rangle$$
$$Z_{dr} = \frac{S_h(n)}{S_v(n)}. \tag{28}$$

The expression (27) demonstrates that the bias is dependent on signal parameters that span three consecutive range gates. Therefore, it is dependent on gradients that these parameters exhibit along range. For the purpose of analysis, it is assumed herein that the reflectivity gradients exert the largest impact on the bias in (27). Thus, assuming all parameters except powers are uniform along three consecutive range gates, the bias in (27) is expressed as

$$\langle \mathrm{BIAS}_X(\hat{Z}_{DR})\rangle \approx \frac{10}{\ln(10)}\left\{G0\left[\mathrm{cpcf}_h + \frac{g_{vv}^2}{g_{hh}^2}\mathrm{cpcf}_v Z_{dr}^{-1}\right] - G1\left[\mathrm{cpcf}_v + \frac{g_{hh}^2}{g_{vv}^2}\mathrm{cpcf}_h Z_{dr}\right]\right.$$
$$+ 2|\rho_{hv}(0)|\left[\frac{g_{vv}}{g_{hh}}\mathrm{cpcf}_v\sqrt{Z_{dr}^{-1}}\cos(2\gamma_{vh}+\phi_{DP}) - \frac{g_{hh}}{g_{vv}}\mathrm{cpcf}_h\sqrt{Z_{dr}}\cos(2\gamma_{hv}-2\gamma_{vv}-\phi_{DP})\right.$$
$$\left.\left. + \sqrt{\mathrm{cpcf}_h\mathrm{cpcf}_v}\left(\frac{g_{vv}}{g_{hh}}G0\sqrt{Z_{dr}^{-1}} - \frac{g_{hh}}{g_{vv}}G1\sqrt{Z_{dr}}\right)\cos(\gamma_{vh}-\gamma_{hv}+\gamma_{vv}+\phi_{DP})\right]\right\}(\mathrm{dB}), \tag{29}$$

where

$$G0 = \frac{S_h(n-1)}{S_h(n)} = \frac{S_v(n-1)}{S_v(n)} = 10^{(-1)^g\times(\mathrm{GRAD\_dB}\times\mathrm{range\_gate}/10)}$$
$$G1 = \frac{S_h(n+1)}{S_h(n)} = \frac{S_v(n+1)}{S_v(n)} = 10^{(-1)^{(g+1)}\times(\mathrm{GRAD\_dB}\times\mathrm{range\_gate}/10)}. \tag{30}$$

In (30) GRAD_dB is the reflectivity gradient (dB km^{-1}) and range gate is the depth of resolution volume (km). The letter g denotes a negative gradient if zero and a positive gradient if one.

To gain a measure of the biases that could be incurred, assume beams are near broadside, where $F_{hh} \approx F_{vv}$, $|F_{hv}| \approx |F_{vh}|$ (i.e., $\mathrm{CPCF}_h = \mathrm{CPCF}_v = \mathrm{CPCF}$), and $\gamma_{vh} \approx \gamma_{hv} \pm \pi$ (Balanis 2005; Bhardwaj and Rahmat-Samii 2014). Under these conditions (29) reduces to

$$\langle \mathrm{BIAS}_X(\hat{Z}_{DR})\rangle \approx \frac{10\mathrm{cpcf}}{\ln(10)}\left\{G0(1+Z_{dr}^{-1}) - G1(1+Z_{dr})\right.$$
$$+ 2|\rho_{hv}(0)|\left[\sqrt{Z_{dr}^{-1}}\cos(2\gamma_{hv}+\phi_{DP}) - \sqrt{Z_{dr}}\cos(2\gamma_{hv}-\phi_{DP})\right.$$
$$\left.\left. - (G0\sqrt{Z_{dr}^{-1}} - G1\sqrt{Z_{dr}})\cos(\phi_{DP})\right]\right\}(\mathrm{dB}). \tag{31}$$

In the SHV mode and for the same conditions as for (31), the bias is (Zrnić et al. 2010)

$$\langle \mathrm{BIAS}_X(\hat{Z}_{DR})\rangle \approx \langle\hat{Z}_{DR}\rangle - \langle\hat{Z}_{DR}^{NX}\rangle$$
$$\approx \frac{20\sqrt{\mathrm{cpcf}}}{\ln(10)}\left[\cos(\gamma_{hv}+\beta) - \frac{|\rho_{hv}(0)|}{\sqrt{Z_{dr}}}\cos(\gamma_{hv}+\phi_{DP}+\beta)\right.$$
$$\left. + \cos(\gamma_{hv}-\beta) - \sqrt{Z_{dr}}|\rho_{hv}(0)|\cos(\gamma_{hv}-\phi_{DP}-\beta)\right](\mathrm{dB}). \tag{32}$$

If no reflectivity gradients are present CPCF = −25 dB, $Z_{dr} = 1$, and $|\rho_{hv}(0)| = 0.99$, (31) indicates that the maximum bias of ±0.0544 occurs if $\gamma_{hv} = \pm\pi/4$, and $\phi_{DP} = \pm\pi/2$. Expression (32) shows that under the same conditions, the maximum positive bias, in SHV mode, of 1.944 occurs if $\gamma_{hv} = \beta = 0$, and $\phi_{DP} = \pi$.

Expressions (27) and (29) demonstrate that Z_{DR} bias is also dependent on the ratio of g_{hh} and g_{vv}. To assess the bounds of $(g_{hh}/g_{vv})^2$, antennas are considered as large assemblies of Hertzian dipoles (Popović and Popović 2000). Then the direction dependence of the Poynting vector for a single dipole oriented along the y axis is proportional to $\sin^2(\phi)$. Assuming $g_{hh} = g_{vv}$ at broadside and the four-face PPPAR, the worst mismatch at $\theta = 90°$ is −6 dB, which occurs when the boresight is at $\phi = \pm 45°$. Following the same rationale, $(g_{hh}/g_{vv})^2 = 6$ dB if the beam is pointed at $\theta = 45°$ and $\phi = 0°$.

To verify the results of the perturbation analysis, the bias was also examined using simulated time series. The bias is estimated as

$$\mathrm{BIAS}_X(\hat{Z}_{DR}) = \frac{10}{K_s}\sum_{k_s=0}^{K_s-1}\log_{10}\left\{\left[\frac{\frac{1}{M}\sum_{m=0}^{M-1}|V_h(n,m,k_s)|^2}{\frac{1}{M}\sum_{m=0}^{M-1}|V_v(n+1,m,k_s)|^2}\right]\Bigg/\left[\frac{\frac{g_{hh}^2}{M}\sum_{m=0}^{M-1}|s_{hh}(n,m,k_s)|^2}{\frac{g_{vv}^2}{M}\sum_{m=0}^{M-1}|s_{vv}(n,m,k_s)|^2}\right]\right\}(\mathrm{dB}), \tag{33}$$

where K_s is the number of simulation runs and the k_s designator denotes the simulated sample number. Note that the bias computed in (29) and (33) is the bias added to the inherent Z_{DR} estimator bias [i.e., bias is present even if copolar gains are matched and cross coupling is not present (Melnikov and Zrnić 2007)] assuming that the bias resulting from the antenna gain mismatch is corrected via calibration.

Using (29) and the simulated time series, the maximum positive and negative cross-coupling biases were found [via a search method using (29)] for a range of reflectivity gradient values if $\mathrm{CPCF}_h = \mathrm{CPCF}_v = -25$ dB and $(g_{hh}/g_{vv})^2$ is 0, 3, and 6 dB for Z_{DR} of 0 and 1 dB (because the bias requirements are the most stringent for Z_{DR} ranging between these two values). Results are presented in Fig. 2. Curves produced for $Z_{DR} = 0$ dB in Fig. 2a imply that if antenna gains in H and V are equal (i.e., $g_{hh} = g_{vv}$), then the Z_{DR} bias falls roughly within ±0.1 dB for reflectivity gradients within ±10 dB km^{-1}. However, the results for antenna gains mismatched to incur a 3-dB difference in received power between the H and V channels indicate an increased bias that exceeds the 0.1-dB value at a reflectivity gradient of about 2 dB km^{-1}. If $(g_{hh}/g_{vv})^2 = 6$ dB, then the bias of 0.1 dB is exceeded along the entire gradient range. Figure 2b shows the same but for $Z_{DR} = 1$ dB. The curves indicate that the increase in Z_{DR} produces a rise in the maximum negative biases and the effect becomes more pronounced as the ratio $(g_{hh}/g_{vv})^2$ increases.

Next, the standard deviation (SD) of differential reflectivity is examined. An assessment of variance using perturbation analysis is given in the appendix. Assuming all parameters except powers to be uniform along three consecutive range gates, the SD is

$$\begin{aligned}\mathrm{SD}_X(\hat{Z}_{DR}) \approx \Bigg\{ & \mathrm{Var}(\hat{Z}_{DR}^{NX}) + \frac{200}{M_I \ln^2(10)}\Bigg[\mathrm{cpcf}_h\frac{S_h(n-1)}{S_h(n)} + \frac{g_{vv}}{g_{hh}}\mathrm{cpcf}_v\frac{S_v(n-1)}{S_h(n)} \\ & + \mathrm{cpcf}_v\frac{S_v(n+1)}{S_v(n)} + \frac{g_{hh}}{g_{vv}}\mathrm{cpcf}_h\frac{S_h(n+1)}{S_v(n)} + 2\sqrt{\mathrm{cpcf}_h\mathrm{cpcf}_v}|\rho_{hv}(0)| \\ & \times\left[\frac{g_{vv}S_h(n-1)}{g_{hh}S_h(n)}\sqrt{Z_{dr}^{-1}} + \frac{g_{hh}S_v(n+1)}{g_{vv}S_v(n)}\sqrt{Z_{dr}}\right]\cos(\gamma_{vv} + \gamma_{hv} - \gamma_{vh} - \phi_{DP})\Bigg]\Bigg\}^{1/2}(\mathrm{dB}).\end{aligned} \tag{34}$$

From (34) it is inferred that SD is dependent on the differential phase and the largest SD occurs if

$$\gamma_{vv} + \gamma_{hv} - \gamma_{vh} = \phi_{DP}. \tag{35}$$

Additionally, standard deviations are computed using simulations as

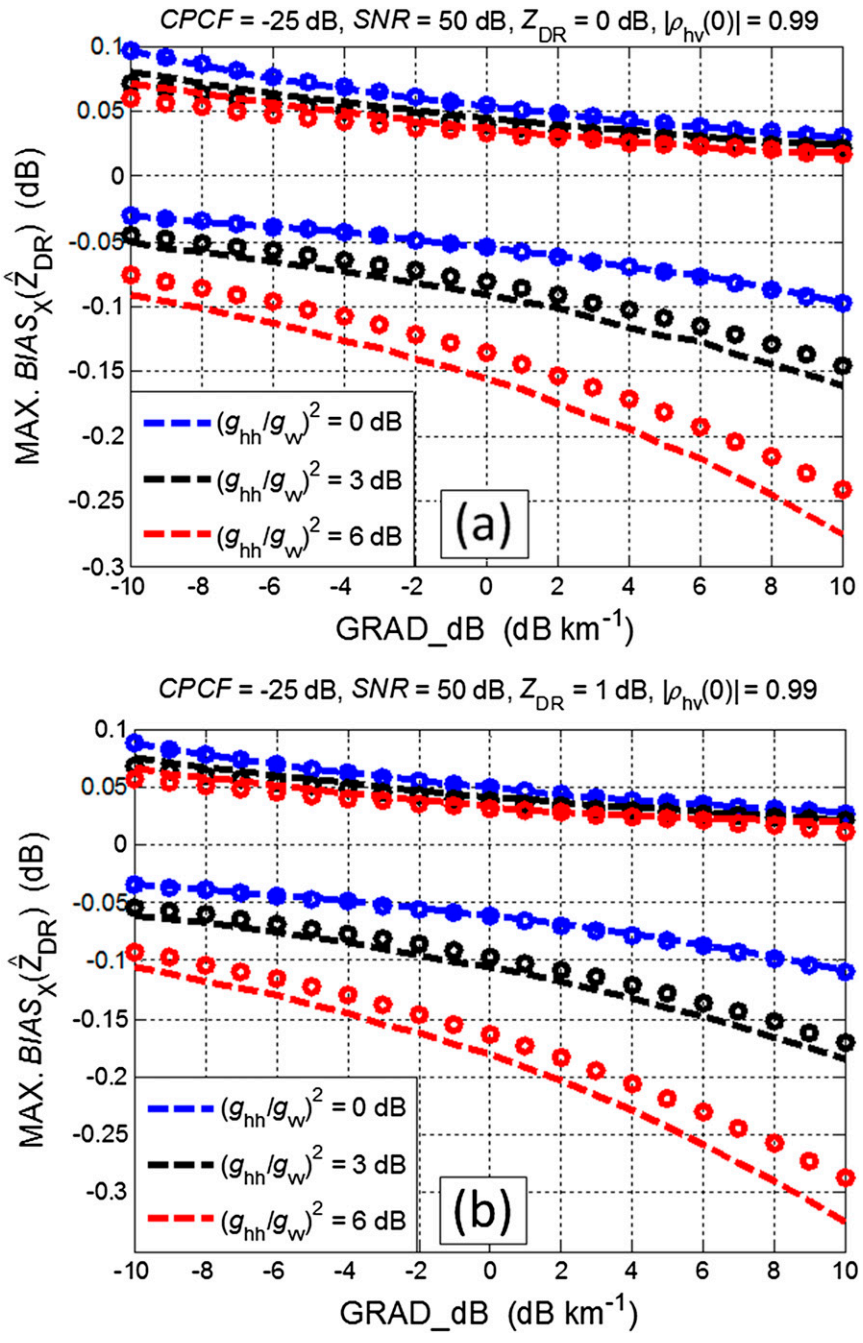

FIG. 2. Positive and negative maximum cross-coupling differential reflectivity bias for M = 16, SNR = 50 dB, and $\mathrm{CPCF_h} = \mathrm{CPCF_v} = \mathrm{CPCF} = -25$ dB obtained using simulations (dashed lines) and perturbation (circles) for a range of GRAD_dB values if (a) Z_{DR} = 0 dB and (b) Z_{DR} = 1 dB.

$$\mathrm{SD}_{\mathrm{X}}(\hat{Z}_{\mathrm{DR}}) = \sqrt{\frac{100}{K_s - 1}\sum_{k_s=0}^{K_s-1}\left\{\log_{10}\left[\frac{\frac{1}{M}\sum_{m=0}^{M-1}|V_{\mathrm{h}}(n,m,k_s)|^2}{\frac{1}{M}\sum_{m=0}^{M-1}|V_{\mathrm{v}}(n+1,m,k_s)|^2}\right] - \frac{1}{K}\sum_{l_s=0}^{K_s-1}\log_{10}\left[\frac{\frac{1}{M}\sum_{m=0}^{M-1}|V_{\mathrm{h}}(n,m,l_s)|^2}{\frac{1}{M}\sum_{m=0}^{M-1}|V_{\mathrm{v}}(n+1,m,l_s)|^2}\right]\right\}^2} \ (\mathrm{dB}). \tag{36}$$

The results of the standard deviation computations for $(g_{\mathrm{hh}}/g_{\mathrm{vv}})^2$ of 0, 3, and 6 dB as functions of reflectivity gradient and differential phase are shown in Figs. 3 and 4 for $M = 16$ and CPCF $= -25$ dB, respectively. The results for standard deviations were produced using (34) and simulations if cross coupling is present but using only simulations if cross coupling is not present (i.e., for SD of $\hat{Z}_{\mathrm{DR}}^{\mathrm{NX}}$). If $g_{\mathrm{hh}} = g_{\mathrm{vv}}$, $Z_{\mathrm{DR}} = 0$ dB, and the reflectivity gradient is 10 dB km^{-1}, the worst standard deviation is about 0.55 dB compared to 0.35 dB when no cross coupling is present (an increase of about 57%) as shown in Fig. 3a. If $g_{\mathrm{hh}} = g_{\mathrm{vv}}$ and $Z_{\mathrm{DR}} = 4$ dB, the cross coupling induces the worst increase in standard deviation of 71% (Fig. 3b). An increased ratio of $(g_{\mathrm{hh}}/g_{\mathrm{vv}})^2$ induces a further rise in SD. The worst standard deviation of about 0.81 dB (an increase of about 231% compared to when no cross coupling is present) occurs if antenna gains are mismatched by 6 dB and the reflectivity gradient is 10 dB km^{-1} at Z_{DR} of 4 dB. Figure 4a and 4b demonstrates that the increase in SD is tightly related to change in ϕ_{DP}.

4. Real data analysis

Next, biases resulting from cross coupling are examined using a dwell (or radial) of time series collected by the KOUN WSR-88D research radar in Norman, Oklahoma. At the time of collection, the radar operated at a PRT of 3.1 ms, which is standard for differential reflectivity measurements during surveillance scans on the WSR-88D at low elevations. These settings yield an unambiguous range (r_a) of 465 km and a Nyquist velocity (v_a) of about 9 m s^{-1}. Hence, no range ambiguities are present. The total number of samples M per radial is 17.

The SNR profile in the H channel is shown in Fig. 5a and the original $\hat{Z}_{\mathrm{DR}}$(WSR-88D) estimates in Fig. 5b. It is assumed herein that the effects of cross-polar fields in WSR-88D are negligible [i.e., $\langle\hat{Z}_{\mathrm{DR}}(\mathrm{WSR\text{-}88D})\rangle = \langle\hat{Z}_{\mathrm{DR}}^{\mathrm{NX}}\rangle$] (Zrnić et al. 2010). The ϕ_{DP} was artificially set to 180° at range $r_0 = 40$ km, which is about 17 km into the storm as shown in Fig. 5c. To emulate cross-polar coupling, the original time series voltages $V_l(m)$ from the H and V channels in WSR-88D were scaled according to the CPCF and introduced into (14) to synthesize two sets of modified time series that emulate cross-polar coupling in the SHV and QSHV modes. Note that in the SHV mode returns, $s'_{\mathrm{hh}}(n, m)$ and $s_{\mathrm{vv}}(n, m)$ are aligned (as opposed to the QSHV mode) so $n - 1$ needs to be replaced by n when the original time series are combined as in (14). Hence, this approach is similar to that used in the previous paragraph to simulate cross-coupling effects except that the real time series from WSR-88D were used in place of the time series generated using the approach described in Zrnić (1975) and Galati and Pavan (1995). In both sets $F_{\mathrm{hh}} = F_{\mathrm{vv}} = 1$, $|F_{\mathrm{hv}}| = |F_{\mathrm{vh}}|$, $\beta = 0°$, and CPCF $= -25$ dB. Phases of the cross-polar patterns are $\gamma_{\mathrm{hv}} = 0°$, $\gamma_{\mathrm{vh}} = \gamma_{\mathrm{hv}} - 180°$ because (32) shows this phase selection leads to maximum positive bias for $\phi_{\mathrm{DP}} = 180°$ in the SHV mode.

In Fig. 5d plots show instantaneous differences ΔZ_{DR} computed as

$$\Delta Z_{\mathrm{DR}} = \hat{Z}_{\mathrm{DR}} - \hat{Z}_{\mathrm{DR}}^{\mathrm{NX}}, \tag{37}$$

where $\hat{Z}_{\mathrm{DR}}$ was obtained from the modified time series and $\hat{Z}_{\mathrm{DR}}^{\mathrm{NX}}$ was computed from the original time series. This difference is an assessment of the bias introduced by the cross coupling. It demonstrates that a CPCF of -25 dB produces an unacceptable additional bias in Z_{DR} estimates if a plain SHV mode is used. The QSHV mode produces an average ΔZ_{DR} of 0.0066 dB in this particular case. This test is similar to the one presented in Zrnić et al. (2014). Both tests demonstrate the capability of the QSHV mode to successfully diminish the bias caused by cross-coupling signals. However, an increase in the fluctuations of ΔZ_{DR} at ranges beyond 50 km further demonstrates that the QSHV mode also introduces a ϕ_{DP}-dependent increase in the standard deviation of differential reflectivity estimates. This is in agreement with the results demonstrated herein using analytical derivations and simulated time series.

5. Summary and conclusions

For polarimetric radars using simultaneous transmission and reception to and from oblate spheroidal

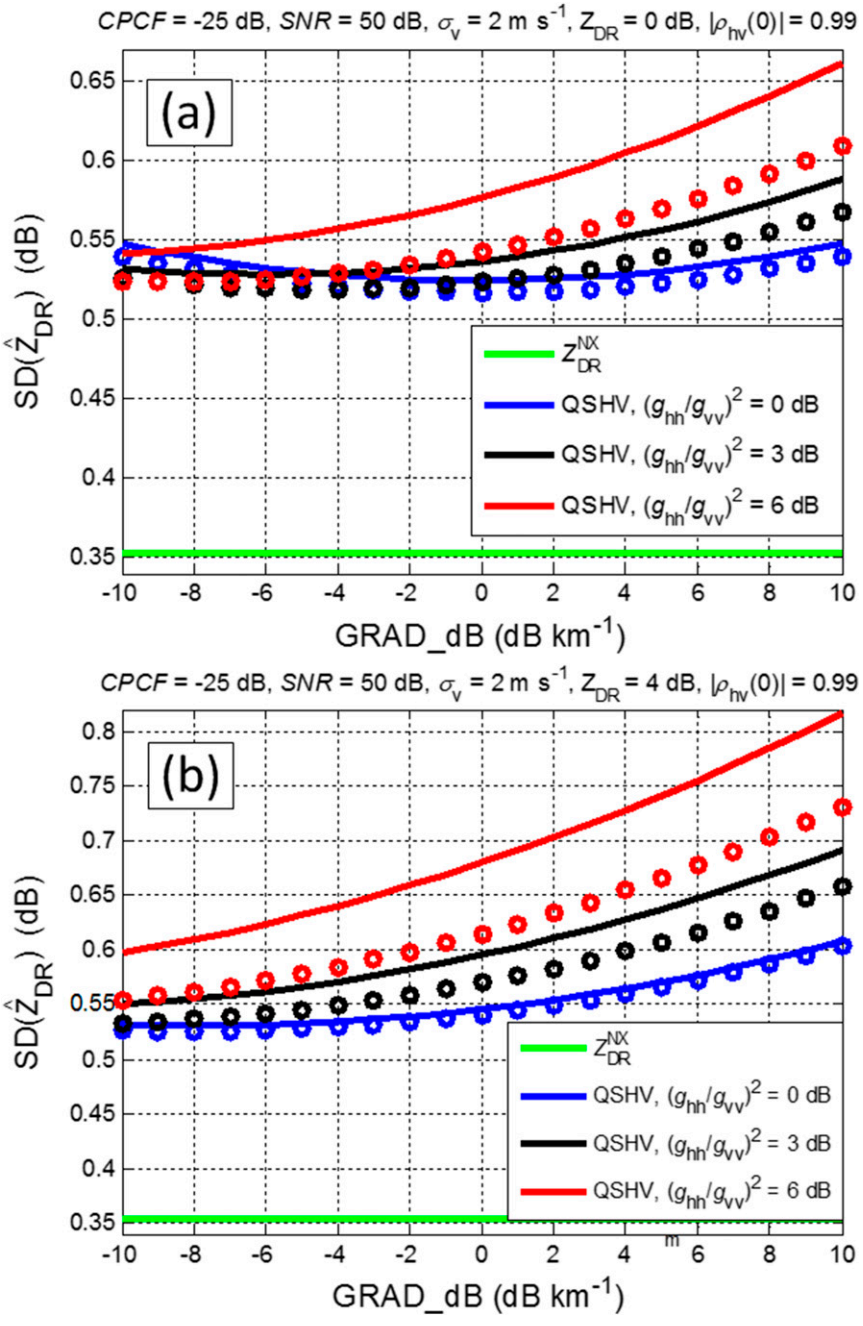

FIG. 3. Maximum differential reflectivity standard deviation for $M = 16$, SNR = 50 dB, and CPCF of −25 dB obtained using simulations (dashed lines) and perturbation (circles) for a range of GRAD_dB values if (a) $Z_{DR} = 0$ dB and (b) $Z_{DR} = 4$ dB.

scatterers all having a vertical axis of symmetry, the power estimate in each of the two channels is a sum of the power from the copolar returns (caused solely by the antenna's copolar radiation fields), the cross-polar returns (caused solely by the cross-polar radiation fields), and the product of the copolar and cross-polar signals (i.e., co/X-pol product). Differences in H and V copolar gains induce bias, defined as copolar Z_{DR} bias, even if there is no cross-polar radiation. The copolar Z_{DR} bias is independent of scatterer properties and must be accounted for via calibration. The powers of antenna-produced cross-polar returns and co/X-pol products in H and V also produce bias in Z_{DR} estimates. This bias is referred to as antenna cross-coupling bias because it is

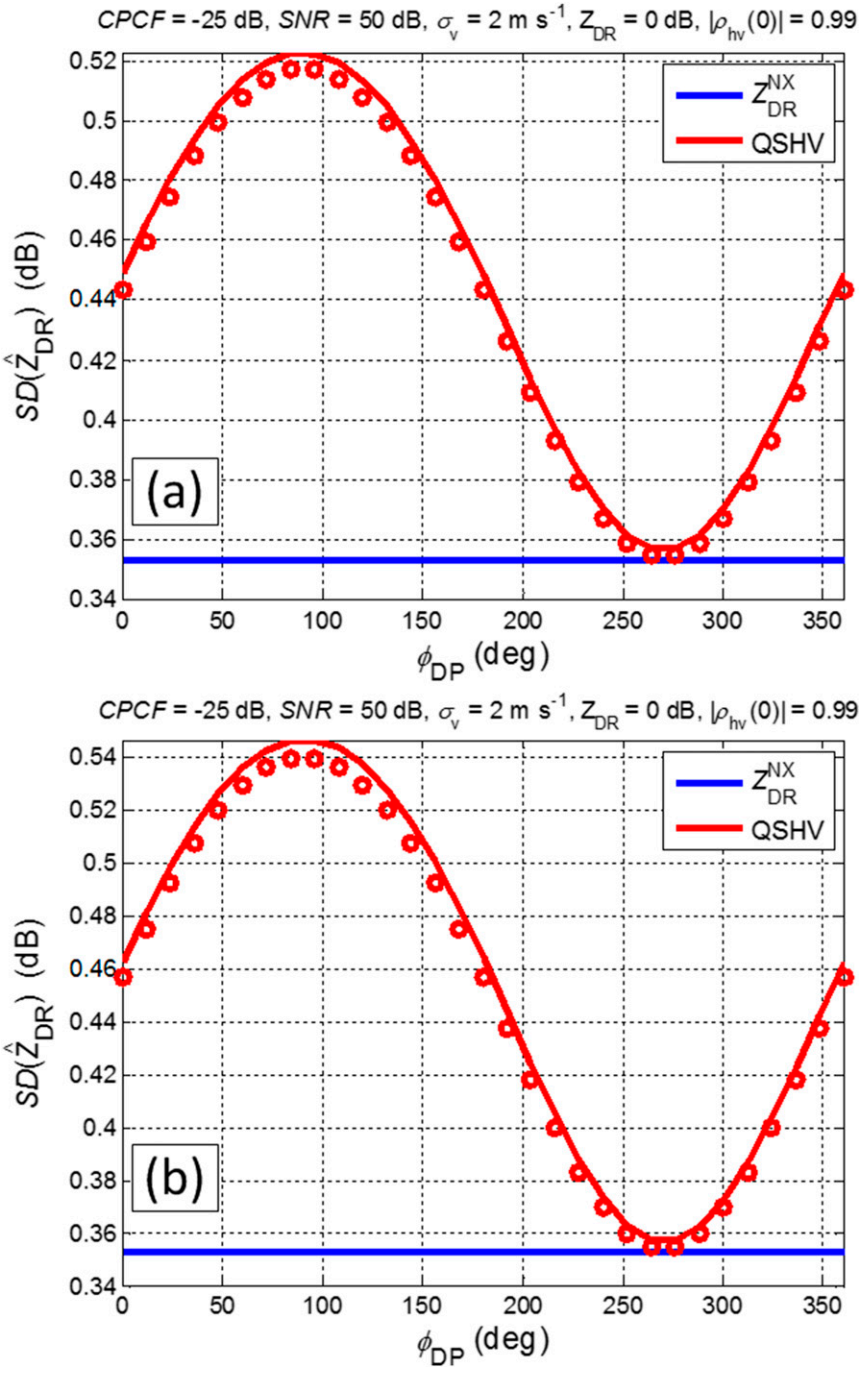

FIG. 4. Maximum differential reflectivity standard deviation for $M = 16$, SNR = 50 dB, and CPCF of −25 dB obtained using simulations (dashed lines) and perturbation (circles) for a range of ϕ_{DP} values when $g_{hh} = g_{vv}$ if (a) GRAD_dB = 0 dB and (b) GRAD_dB = 10 dB.

caused by the cross-polar fields. Contrary to copolar bias, the cross-coupling bias depends on the scatterer properties and is therefore difficult to account for using calibration. The co/X-pol product is the largest contributor to cross-coupling Z_{DR} bias.

To diminish Z_{DR} bias resulting from the co/X-pol product, the use of time multiplexing was investigated. In such an approach, the V transmitter port is energized after the H port or vice versa so that the co/X-pol term is zero in the mean as instantaneous power estimates are

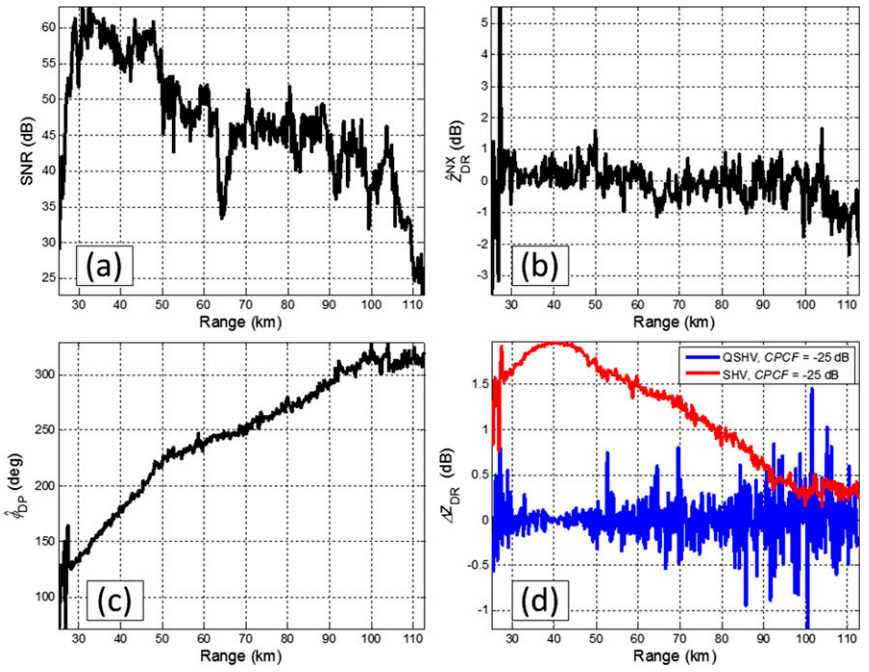

FIG. 5. Assessment of cross-coupling differential reflectivity bias using a radial of real time series with $M = 17$: (a) SNR, (b) $\hat{Z}_{DR}^{NX}$, (c) $\hat{\phi}_{DP}$, and (d) ΔZ_{DR} range profiles.

averaged. Thus, this approach reduces the co/X-pol term but not the product of cross-polar signals (i.e., second-order effects). But this incurs bias in Z_{DR} estimates that is typically significantly smaller than that induced by the co/X-pol product.

In this paper, the resultant quality of cross-polar isolation, produced by this approach, in terms of differential reflectivity bias and standard deviation was evaluated using perturbation analysis and simulated as well as time series data collected using WSR-88D research radar. The analysis was conducted for parameters typical of a long PRT surveillance scan on the WSR-88D because such capability is expected from the future PPAR.

The assessment via the perturbation analysis and the simulated time series has indicated that the inherent cross-polar isolation of −25 dB in both H and V coupled with the time-multiplexing produced the worst cross-coupling differential reflectivity bias of about −0.055 dB if antenna gains in the H and V channels were the same with no reflectivity gradients at $Z_{DR} = 0$ dB. If the difference in antenna gains is 6 dB, the worst-case Z_{DR} bias increases to about −0.15 dB. The presence of reflectivity gradients in range increased the bias so that at a gradient of 10 dB km^{-1}, the bias was about −0.1 dB if antenna gains were matched and −0.27 dB for antenna gains mismatched by 6 dB. This demonstrates that while the application of time multiplexing mitigates cross-coupling Z_{DR} bias (by removing the co/X-pol product), it is sensitive to reflectivity gradients in range and antenna gain mismatch, which diminishes the efficacy of this approach.

Furthermore, when assessing the acceptable level of cross-coupling bias in Z_{DR} estimates, the fact that it is compounded with the copolar bias needs to be taken into account. If the copolar bias is accounted for by Z_{DR} calibration, its accuracy needs to be such that if its error is constructively added to the worst cross-coupling bias, the resulting bias remains within the prescribed limits (e.g., 0.1 dB). Thus, as the cross coupling incurs less bias, the requirements for the accuracy of Z_{DR} calibration become less stringent, and vice versa.

A comparison to the SHV mode with no cross coupling revealed a ϕ_{DP}-dependent increase in standard deviation of differential reflectivity estimates obtained from time-multiplexed returns. For matched antenna gains and a differential reflectivity of 4 dB, the worst increase in standard deviation ranges between 51% and 71% for reflectivity gradients of ±10 dB km^{-1}. If antenna gains are mismatched by 6 dB, the worst standard deviation increase was measured to be between 71% and 231%.

An additional evaluation of the phase codes' suppression capability was conducted using one radial of time series collected by the WRS-88D radar. Radars in the WRS-88D network use parabolic antennas and are deemed to provide sufficient cross-polar isolation so that the influence of cross-polar coupling can be neglected. To emulate the cross-polarization effect, the original

time series in the horizontal channel were artificially contaminated by returns from the vertical channel and vice versa. The coupling parameters were set so that the worst differential reflectivity bias was produced for the 180° differential phase. Emulation in case of −25 dB overall cross-coupling suppression with no time-multiplexing produced visible differences compared to the original differential reflectivity. Application of time multiplexing with cross-coupling suppression of −25 dB yielded the differential reflectivity values with an average bias of 0.0066 dB but with a visible increase in standard deviation. This further corroborated the results from analytical derivations and simulations.

Acknowledgments. The author would like to thank Dr. Dušan S. Zrnić, who introduced the authors to the issues facing PPAR and provided valuable comments and guidance that enhanced this work Also, the author would like to thank Dr. Bradley Isom for providing comments that improved the manuscript. Funding was provided by NOAA/Office of Oceanic and Atmospheric Research under NOAA–University of Oklahoma Cooperative Agreement NA11OAR4320072, U.S. Department of Commerce.

APPENDIX

Z_{DR} Variance Derivation

In this appendix the variance of Z_{DR} is studied. Given (26), the variance of Z_{DR} is approximately

$$\mathrm{Var}(\hat{Z}_{DR}) \approx \mathrm{Var}(\hat{Z}_{DR}^{NX}) + \frac{20}{\ln(10)}\left[\mathrm{Cov}\left(\hat{Z}_{DR}^{NX}, \frac{\delta\hat{P}_h}{\hat{S}_h^{NX}}\right) - \mathrm{Cov}\left(\hat{Z}_{DR}^{NX}, \frac{\delta\hat{P}_v}{\hat{S}_v^{NX}}\right)\right] + \frac{100}{\ln^2(10)}\left[\mathrm{Var}\left(\frac{\delta\hat{P}_h}{\hat{S}_h^{NX}}\right) + \mathrm{Var}\left(\frac{\delta\hat{P}_v}{\hat{S}_v^{NX}}\right) - 2\,\mathrm{Cov}\left(\frac{\delta\hat{P}_h}{\hat{S}_h^{NX}}, \frac{\delta\hat{P}_v}{\hat{S}_v^{NX}}\right)\right]. \quad \text{(A1)}$$

In the case when time multiplexing is used, the largest number of returns in $\delta\hat{P}_h$ are from a V_6 volume located at $r - c\tau/2$, whereas in $\delta\hat{P}_v$ most returns are from a V_6 volume at $r + c\tau/2$. This implies that

$$\mathrm{Var}\left(\frac{\delta\hat{P}_h}{\hat{S}_h^{NX}}\right) + \mathrm{Var}\left(\frac{\delta\hat{P}_v}{\hat{S}_v^{NX}}\right) \gg 2\,\mathrm{Cov}\left(\frac{\delta\hat{P}_h}{\hat{S}_h^{NX}}, \frac{\delta\hat{P}_v}{\hat{S}_v^{NX}}\right). \quad \text{(A2)}$$

Furthermore, it was found that

$$\mathrm{Cov}\left(\hat{Z}_{DR}^{NX}, \frac{\delta\hat{P}_h}{\hat{S}_h^{NX}}\right) = \mathrm{Cov}\left(\hat{Z}_{DR}^{NX}, \frac{\delta\hat{P}_v}{\hat{S}_v^{NX}}\right). \quad \text{(A3)}$$

Hence, (A1) reduces to

$$\mathrm{Var}(\hat{Z}_{DR}) \approx \mathrm{Var}(\hat{Z}_{DR}^{NX}) + \frac{100}{\ln^2(10)}\left[\mathrm{Var}\left(\frac{\delta\hat{P}_h}{\hat{S}_h^{NX}}\right) + \mathrm{Var}\left(\frac{\delta\hat{P}_v}{\hat{S}_v^{NX}}\right)\right]. \quad \text{(A4)}$$

By development into a Taylor series, the approximate variance of a ratio is

$$\mathrm{Var}\left(\frac{x}{y}\right) \approx \frac{\mathrm{Var}(x)}{\langle y\rangle^2} - 2\frac{\langle x\rangle}{\langle y\rangle^3}\,\mathrm{Cov}(x,y) + \frac{\langle x\rangle^2}{\langle y\rangle^4}\,\mathrm{Var}(y), \quad \text{(A5)}$$

where x and y are random variables. Using (A5) the variance becomes

$$\mathrm{Var}(\hat{Z}_{DR}) \approx \mathrm{Var}(\hat{Z}_{DR}^{NX}) + \frac{100}{\ln^2(10)}\left[\frac{\mathrm{Var}(\delta\hat{P}_h)}{\langle\hat{S}_h^{NX}\rangle^2} + \frac{\langle\delta\hat{P}_h\rangle^2}{\langle\hat{S}_h^{NX}\rangle^4}\mathrm{Var}(\hat{S}_h^{NX}) + \frac{\mathrm{Var}(\delta\hat{P}_v)}{\langle\hat{S}_v^{NX}\rangle^2} + \frac{\langle\delta\hat{P}_v\rangle^2}{\langle\hat{S}_v^{NX}\rangle^4}\mathrm{Var}(\hat{S}_v^{NX}) - 2\frac{\langle\delta\hat{P}_h\rangle}{\langle\hat{S}_h^{NX}\rangle^3}\mathrm{Cov}(\delta\hat{P}_h, \hat{S}_h^{NX}) - 2\frac{\langle\delta\hat{P}_v\rangle}{\langle\hat{S}_v^{NX}\rangle^3}\mathrm{Cov}(\delta\hat{P}_v, \hat{S}_v^{NX})\right]. \quad \text{(A6)}$$

Next, the numerator of the first term in the brackets is determined as

$$\mathrm{Var}(\delta\hat{P}_h) = \mathrm{Var}(\delta\hat{P}_{1h}) + \mathrm{Var}(\delta\hat{P}_{2h}) + 2\,\mathrm{Cov}(\delta\hat{P}_{1h}, \delta\hat{P}_{2h}). \quad \text{(A7)}$$

Because $\delta\hat{P}_{2h}$ contains products in which F_{hh} or F_{vv} appear on the first power, it is the largest contributor to the sum in (A7). Thus, assuming all parameters except powers to be uniform along three consecutive range gates, (A7) is

$$\mathrm{Var}(\delta\hat{P}_{\mathrm{h}}) \approx \frac{2S_{\mathrm{h}}^2(n)}{M_I}\left[g_{\mathrm{hh}}^4 \mathrm{cpcf}_{\mathrm{h}}\frac{S_{\mathrm{h}}(n-1)}{S_{\mathrm{h}}(n)} + g_{\mathrm{hh}}^3 g_{\mathrm{vv}}\mathrm{cpcf}_{\mathrm{v}}\frac{S_{\mathrm{v}}(n-1)}{S_{\mathrm{h}}(n)} + 2g_{\mathrm{hh}}^3 g_{\mathrm{vv}}\sqrt{\mathrm{cpcf}_{\mathrm{h}}\mathrm{cpcf}_{\mathrm{v}}}\,\frac{S_{\mathrm{h}}(n-1)}{S_{\mathrm{h}}(n)}\sqrt{Z_{\mathrm{dr}}^{-1}}|\rho_{\mathrm{hv}}(0)|\,\mathrm{Cos}(\gamma_{\mathrm{vv}}+\gamma_{\mathrm{hv}}-\gamma_{\mathrm{vh}}-\phi_{\mathrm{DP}})\right]. \quad \text{(A8)}$$

Using the same rationale the variance for the V channel is

$$\mathrm{Var}(\delta\hat{P}_{\mathrm{v}}) \approx \frac{2S_{\mathrm{v}}^2(n)}{M_I}\left[g_{\mathrm{vv}}^4 \mathrm{cpcf}_{\mathrm{v}}\frac{S_{\mathrm{v}}(n+1)}{S_{\mathrm{v}}(n)} + g_{\mathrm{vv}}^3 g_{\mathrm{hh}}\mathrm{cpcf}_{\mathrm{h}}\frac{S_{\mathrm{h}}(n+1)}{S_{\mathrm{v}}(n)} + 2g_{\mathrm{vv}}^2 g_{\mathrm{hh}}\sqrt{\mathrm{cpcf}_{\mathrm{h}}\mathrm{cpcf}_{\mathrm{v}}}\,\frac{S_{\mathrm{v}}(n+1)}{S_{\mathrm{v}}(n)}\sqrt{Z_{\mathrm{dr}}}|\rho_{\mathrm{hv}}(0)|\,\cos(\gamma_{\mathrm{vv}}+\gamma_{\mathrm{hv}}-\gamma_{\mathrm{vh}}-\phi_{\mathrm{DP}})\right]. \quad \text{(A9)}$$

The expressions in (A8) and (A9) are the largest contributors in brackets in (A6). Hence,

$$\begin{aligned}\mathrm{Var}(\hat{Z}_{\mathrm{DR}}) \approx \mathrm{Var}(\hat{Z}_{\mathrm{DR}}^{\mathrm{NX}}) + \frac{200}{M_I \ln^2(10)}\Bigg[&g_{\mathrm{hh}}^2\mathrm{cpcf}_{\mathrm{h}}\frac{S_{\mathrm{h}}(n-1)}{S_{\mathrm{h}}(n)} + g_{\mathrm{hh}}g_{\mathrm{vv}}\mathrm{cpcf}_{\mathrm{v}}\frac{S_{\mathrm{v}}(n-1)}{S_{\mathrm{h}}(n)}\\ &+ 2g_{\mathrm{hh}}g_{\mathrm{vv}}\sqrt{\mathrm{cpcf}_{\mathrm{h}}\mathrm{cpcf}_{\mathrm{v}}}\,\frac{S_{\mathrm{h}}(n-1)}{S_{\mathrm{h}}(n)}\sqrt{Z_{\mathrm{dr}}^{-1}}|\rho_{\mathrm{hv}}(0)|\cos(\gamma_{\mathrm{vv}}+\gamma_{\mathrm{hv}}-\gamma_{\mathrm{vh}}-\phi_{\mathrm{DP}})\\ &+ g_{\mathrm{vv}}^2\mathrm{cpcf}_{\mathrm{v}}\frac{S_{\mathrm{v}}(n+1)}{S_{\mathrm{v}}(n)} + g_{\mathrm{hh}}g_{\mathrm{vv}}\mathrm{cpcf}_{\mathrm{h}}\frac{S_{\mathrm{h}}(n+1)}{S_{\mathrm{v}}(n)}\\ &+ 2g_{\mathrm{hh}}g_{\mathrm{vv}}\sqrt{\mathrm{cpcf}_{\mathrm{h}}\mathrm{cpcf}_{\mathrm{v}}}\,\frac{S_{\mathrm{v}}(n+1)}{S_{\mathrm{v}}(n)}\sqrt{Z_{\mathrm{dr}}}|\rho_{\mathrm{hv}}(0)|\cos(\gamma_{\mathrm{vv}}+\gamma_{\mathrm{hv}}-\gamma_{\mathrm{vh}}-\phi_{\mathrm{DP}})\Bigg]. \quad \text{(A10)}\end{aligned}$$

REFERENCES

Balanis, C. A., 2005: *Antenna Theory*. John Willey & Sons, 1047 pp.

Bhardwaj, S., and Y. Rahmat-Samii, 2014: Revisiting the generation of cross-polarization in rectangular patch antennas: A near-field approach. *IEEE Antennas Propag. Mag.*, **56**, 14–38, doi:10.1109/MAP.2014.6821758.

Chandrasekar, V., and R. J. Keeler, 1993: Antenna pattern analysis and measurements for multiparameter radars. *J. Atmos. Oceanic Technol.*, **10**, 674–683, doi:10.1175/1520-0426(1993)010<0674:APAAMF>2.0.CO;2.

——, and N. Bharadwaj, 2009: Orthogonal channel coding for simultaneous co- and cross-polarization measurements. *J. Atmos. Oceanic Technol.*, **26**, 45–56, doi:10.1175/2008JTECHA1101.1.

Crain, G. E., and D. Staiman, 2007: Polarization selection for phased array weather radar. *23rd Conf. on Interactive Information Processing Systems*, San Antonio, TX, Amer. Meteor. Soc., 7.7. [Available online at https://ams.confex.com/ams/87ANNUAL/techprogram/paper_118019.htm.]

Doviak, R. J., and D. S. Zrnić, 1993: *Doppler Radar and Weather Observations*. Academic Press, 562 pp.

Galati, G., and G. Pavan, 1995: Computer simulation of weather radar signals. *Simul. Pract. Theory*, **3**, 17–44, doi:10.1016/0928-4869(95)00009-I.

Galletti, M., D. S. Zrnić, and P. Goelz, 2014: Eigenvalue signal processing for weather radar polarimetry: Removing the bias induced by antenna coherent cross-channel coupling. *IEEE Trans. Geosci. Remote Sens.*, **52**, 7965–7707, doi:10.1109/TGRS.2014.2316821.

Giuli, D., M. Fossi, and L. Facheris, 1993: Radar target scattering matrix measurement through orthogonal signals. *IEE Proc. Radar Signal Process.*, **140F**, 233–242, doi:10.1049/ip-f-2.1993.0033.

Heinselman, P. M., and S. M. Torres, 2011: High-temporal-resolution capabilities of the National Weather Radar Testbed Phased-Array Radar. *J. Appl. Meteor. Climatol.*, **50**, 579–593, doi:10.1175/2010JAMC2588.1.

Hubbert, J. C., V. N. Bringi, and D. Brunkow, 2003: Studies of the polarimetric covariance matrix. Part I: Calibration methodology. *J. Atmos. Oceanic Technol.*, **20**, 696–706, doi:10.1175/1520-0426(2003)20<696:SOTPCM>2.0.CO;2.

Ice, R. L., A. K. Heck, J. G. Cunningham, and W. D. Zittel, 2014: Challenges of polarimetric weather radar calibration. *Extended Abstracts, Eighth European Conf. on Radar in Meteorology and Hydrology (ERAD)*, Garmisch-Partenkirchen, Germany, DWD and DLR, 8.1. [Available online at http://www.roc.noaa.gov/wsr88d/PublicDocs/Publications/PolarWX_Calibration_Eng_Challenges_Ice_radar2013_rv2.pdf].

Ivić, I. R., 2013: Analysis of cross-polar coupling suppression using phase and frequency modulation within the radar pulse. National Severe Storms Laboratory White Paper, 29 pp. [Available online at http://www.ofcm.noaa.gov/wg-mpar/references/nswrc/Analysis%20of%20coupling%20supression%20using%20phase%20codes.pdf.]

Jones, E. M. T., 1954: Paraboloid reflector and hyperboloid lens antennas. *Trans. IRE Prof. Group Antennas Propag.*, **2**, 119–127, doi:10.1109/T-AP.1954.27984.

Knapp, E. J., J. Salazar, R. H. Medina, A. Krishnamurthy, and R. Tessier, 2011: Phase-tilt radar antenna array. *2011 41st European Microwave Conference (EuMc 2011)*, IEEE, 1055–1058.

Lei, L., G. Zhang, R. J. Doviak, and S. Karimkashi, 2015: Comparison of theoretical biases in estimating polarimetric properties of precipitation with weather radar using parabolic reflector, or planar and cylindrical arrays. *IEEE Trans. Geosci. Remote Sens.*, **53**, 4313–4327, doi:10.1109/TGRS.2015.2395714.

Ludwig, A., 1973: The definition of cross polarization. *IEEE Trans. Antennas Propag.*, **21**, 116–117, doi:10.1109/TAP.1973.1140406.

McCarroll, C., and D. McLaughlin, 2012: Weather radar research in Australia: Addressing the need for faster, more accurate weather warnings. Raytheon Technology Today, 2, 12–14.

Melnikov, V. M., and D. S. Zrnić, 2007: Autocorrelation and cross-correlation estimators of polarimetric variables. *J. Atmos. Oceanic Technol.*, **24**, 1337–1350, doi:10.1175/JTECH2054.1.

Oguchi, T., 1983: Electromagnetic wave propagation and scattering in rain and other hydrometeors. *Proc. IEEE*, **71**, 1029–1078, doi:10.1109/PROC.1983.12724.

Perera, S., Y. Pan, Y. Zhang, X. Yu, D. Zrnić, and R. J. Doviak, 2013: A fully reconfigurable polarimetric phased array antenna testbed. *Int. J. Antennas Propag.*, **2014**, 439606, doi:10.1155/2014/439606.

Popović, Z., and B. D. Popović, 2000: *Introductory Electromagnetics*. Prentice Hall, 557 pp.

Sachidananda, M., and D. S. Zrnić, 1985: Z_{DR} measurement considerations for a fast scan capability radar. *Radio Sci.*, **20**, 907–922, doi:10.1029/RS020i004p00907.

——, and ——, 1986: Recovery of spectral moments from overlaid echoes in a Doppler weather radar. *IEEE Trans. Geosci. Remote Sens.*, **GE-24**, 751–764, doi:10.1109/TGRS.1986.289624.

Salazar, J. L., E. J. Knapp, and D. J. McLaughlin, 2010: Dual-polarization performance of the phased-tilt antenna array in a casa dense network radar. *2010 IEEE International Geoscience and Remote Sensing Symposium (IGARSS): Proceedings*, IEEE, 3470–3473, doi:10.1109/IGARSS.2010.5650310.

Stagliano, J. J., Jr., R. J. Helvin, L. J. Alford, and D. Nelson, 2006: Measuring the linear depolarization ratio simultaneously with the other polarimetric variables. *Proc. Fourth European Conf. on Radar in Meteorology and Hydrology*, Barcelona, Spain, Servei Meteorologic de Catalunya, 2.5. [Available online at http://www.crahi.upc.edu/ERAD2006/proceedingsMask/00022.pdf.]

——, J. L. Alford, J. R. Hevlin, and D. A. Nelson, 2009: Phase shifted transmitted signals in a simultaneous dual polarization weather system. U.S. Patent No.7,551,1232 B2, filed 22 March 2006, and issued 23 June 2009.

Wang, Y., and V. Chandrasekar, 2006: Polarization isolation requirements for linear dual-polarization weather radar in simultaneous transmission mode of operation. *IEEE Trans. Geosci. Remote Sens.*, **44**, 2019–2028, doi:10.1109/TGRS.2006.872138.

Zhang, G., R. J. Doviak, D. S. Zrnić, J. Crain, D. Staiman, and Y. Al-Rashid, 2009: Phased array radar polarimetry for weather sensing: A theoretical formulation for bias corrections. *IEEE Trans. Geosci. Remote Sens.*, **47**, 3679–3689, doi:10.1109/TGRS.2009.2029332.

——, ——, ——, R. Palmer, L. Lei, and Y. Al-Rashid, 2011: Polarimetric phased array radar for weather measurement: A planar or cylindrical configuration? *J. Atmos. Oceanic Technol.*, **28**, 63–73, doi:10.1175/2010JTECHA1470.1.

Zrnić, D. S., 1975: Simulation of weatherlike Doppler spectra and signals. *J. Appl. Meteor.*, **14**, 619–620, doi:10.1175/1520-0450(1975)014<0619:SOWDSA>2.0.CO;2.

——, V. M. Melnikov, and J. K. Carter, 2006: Calibrating differential reflectivity on WSR-88D. *J. Atmos. Oceanic Technol.*, **23**, 944–951, doi:10.1175/JTECH1893.1.

——, and Coauthors, 2007: Agile-beam phased array radar for weather observations. *Bull. Amer. Meteor. Soc.*, **88**, 1753–1766, doi:10.1175/BAMS-88-11-1753.

——, R. J. Doviak, G. Zhang, and R. V. Ryzhkov, 2010: Bias in differential reflectivity due to cross-coupling through the radiation patterns of polarimetric weather radars. *J. Atmos. Oceanic Technol.*, **27**, 1624–1637, doi:10.1175/2010JTECHA1350.1.

——, G. Zhang, and R. J. Doviak, 2011: Bias correction and Doppler measurement for polarimetric phased-array radar. *IEEE Trans. Geosci. Remote Sens.*, **49**, 843–853, doi:10.1109/TGRS.2010.2057436.

——, V. M. Melnikov, and R. J. Doviak, 2012: Issues and challenges for polarimetric measurement of weather with an agile beam phased array radar. NOAA/NSSL Rep., 117 pp. [Available online at http://www.nssl.noaa.gov/publications/mpar_reports/MPAR-WEB_RPT-1_071412-7_May_2_2013_wo_comments.pdf.]

——, R. J. Doviak, V. M. Melnikov, and I. R. Ivić, 2014: Signal design to suppress coupling in the polarimetric phased array radar. *J. Atmos. Oceanic Technol.*, **31**, 1063–1077, doi:10.1175/JTECH-D-13-00037.1.